

Observable gravitational waves and ΔN_{eff} with global lepton number symmetry and dark matter

Debasish Borah,^{1,*} Nayan Das,^{1,†} and Rishav Roshan^{2,‡}

¹*Department of Physics, Indian Institute of Technology Guwahati, Assam 781039, India*

²*School of Physics and Astronomy, University of Southampton,
Southampton SO17 1BJ, United Kingdom*

Abstract

We study the possibility of testing a dark matter (DM) scenario embedded in a global lepton number symmetry $U(1)_L$ via gravitational waves (GW) and cosmic microwave background (CMB) observations. The spontaneous breaking of $U(1)_L$ symmetry generates the seesaw scale as well as DM mass dynamically. The (pseudo) Nambu-Goldstone boson, known as majoron, acquires non-zero mass due to soft symmetry breaking terms of quadratic type in the scalar potential, which eventually breaks $U(1)_L$ to its Z_2 subgroup. The spontaneous symmetry breaking, which effectively breaks Z_2 , leads to the formation of domain walls (DW), posing a threat to successful cosmology, if allowed to dominate. As gravity does not respect any global symmetries, we consider higher dimensional operators suppressed by the scale of quantum gravity (QG) namely, Λ_{QG} which introduces the required bias leading to DW annihilation and emission of stochastic gravitational waves (GW) observable at near future experiments. The same operators also lead to decay of DM bringing interesting indirect detection aspects. While DM is produced non-thermally via scalar portal interactions, light majoron can give rise to additional ΔN_{eff} within reach of future CMB experiments.

*Electronic address: dborah@iitg.ac.in

†Electronic address: nayan.das@iitg.ac.in

‡Electronic address: r.roshan@soton.ac.uk

I. INTRODUCTION

Observations of non-zero neutrino mass and mixing, dark matter (DM) and baryon asymmetry of the Universe (BAU) [1, 2] have emerged as clear signs of beyond standard model (BSM) physics. While non-zero neutrino mass and mixing can be explained within the framework of canonical seesaw mechanisms like type-I seesaw [3–8], particle DM scenarios can be broadly categorised into thermal and non-thermal DM depending upon their production mechanisms. Among thermal and non-thermal DM scenarios, the weakly interacting massive particle (WIMP) and feebly interacting massive particle (FIMP), respectively, have been studied extensively in the literature. Recent reviews of WIMP and FIMP can be found in [9] and [10] respectively. Similarly, popular BSM scenarios to explain BAU can be categorized into baryogenesis [11, 12] or leptogenesis [13]. Interestingly, leptogenesis can be realised within most of the seesaw frameworks where one or more of the heavy particles introduced for seesaw origin of neutrino mass can also be responsible for generating a non-zero lepton asymmetry to be converted into BAU later by electroweak sphalerons [14].

In spite of having several motivations for BSM physics mentioned above, none of the experiments across different frontiers have observed any convincing signs of it so far. Canonical seesaw models consistent with neutrino mass and leptogenesis typically have a very high scale for new physics, away from direct experimental reach. On the other hand, WIMP DM has not shown up in direct search experiments either [15]. This might be indicative of the fact that DM is either feebly coupled or interact with the standard model (SM) particles via superheavy mediators. Such null results at DM search or other particle physics experiments searching for BSM physics have also motivated the search for complementary probes at other experiments. For example, some recent attempts have focused on probing high scale seesaw via stochastic gravitational wave (GW) observations [16–28]. The particle physics scenarios explored in these works considered the presence of additional symmetries whose spontaneous breaking not only lead to the dynamical generation of seesaw scale but also leads to the generation of stochastic GW from topological defects like cosmic strings [16–19, 26], domain walls [20, 27, 29–33] or from bubbles generated at first order phase transition [21–25, 28]. GW observations has also been used to probe even higher scales than seesaw, where quantum gravity (QG) effects can become important [34–36]. In these works, the QG effects on explicit global discrete symmetry breaking was considered in the context of

domain wall formation from spontaneous discrete symmetry breaking and consequent GW emission. The authors of [34, 35] also considered the impact of such QG effects on decay of DM which is stabilised by discrete symmetry at renormalisable level.

Motivated by these, we consider a global $U(1)$ symmetry related to the seesaw scale and DM stability and study QG effects leading to stochastic GW and DM decay. Connection to lepton sector and seesaw becomes natural if this Abelian global symmetry is identified as the global lepton number symmetry $U(1)_L$. In the simplest realisation of seesaw, the spontaneous breaking of $U(1)_L$ generates the right handed neutrino (RHN) masses or the seesaw scale dynamically. The same breaking also results in a massless Nambu-Goldstone (NG) boson, known as the majoron [37–40]. Majoron can acquire a non-zero mass from explicit $U(1)_L$ breaking mass terms. When the singlet scalar responsible for breaking $U(1)_L$ spontaneously acquires a non-zero vacuum expectation value (VEV), it essentially breaks a Z_2 symmetry, remnant from $U(1)_L$ after explicit $U(1)_L$ breaking mass terms are included. Even without such explicit symmetry breaking terms, $U(1)_L$ is anomalous in the SM and broken to Z_3 by non-perturbative effects [41, 42]¹. Spontaneous breaking of discrete symmetries like Z_2 leads to the formation of domain walls (DW) [29, 30, 44–46], which can overclose the Universe, if allowed to dominate². We then consider higher dimensional operators suppressed by QG scale as bias leading to disappearance of DW thereby generating stochastic GW signal detectable at ongoing and future experiments. We consider a Dirac fermion having chiral transformation under $U(1)_L$ to be the DM which remains accidentally stable even after $U(1)_L$ or Z_2 breaking, unlike earlier works [34, 35] where a separate Z_2 symmetry was introduced for DM stability. The $U(1)_L$ global symmetry therefore, generates the scale of seesaw, DM mass, ensures the stability of DM and also leads to DW formation in the presence of Z_2 -preserving explicit $U(1)_L$ breaking terms generating majoron mass. The higher dimensional operators suppressed by QG scale can however, lead to DM decay opening up some indirect detection prospects. We discuss the details of DM which interacts with the SM via singlet scalar portal, and the effects of QG scale suppressed operators on GW emission from DW and on DM phenomenology. The RHNs not only generate light neutrino masses via seesaw

¹ See [42, 43] for non-minimal majoron models without domain walls.

² Spontaneous breaking of global $U(1)_L$ can also lead to formation of topological defects known as cosmic strings [47]. However, GW emission remains suppressed compared to particle emission from global strings [48].

Fields	$SU(2)_L \times U(1)_Y \times U(1)_L$ charge
χ_L	$(1, 0, Q_L)$
χ_R	$(1, 0, Q_L + 2)$
N_R	$(1, 0, 1)$
ℓ_L	$(2, -\frac{1}{2}, 1)$
ℓ_R	$(1, -1, 1)$
H	$(2, \frac{1}{2}, 0)$
Φ	$(1, 0, -2)$

TABLE I: Relevant field content of the model.

mechanism, but can also generate the baryon asymmetry of the Universe via leptogenesis [13]. The emergence of Z_2 symmetry from a global $U(1)_L$, effects of QG on DW and DM decay, the presence of the pseudo NG boson or majoron bring complementary detection prospects at particle physics, gravitational waves as well as cosmology based experiments.

This paper is organised as follows. In section II, we discuss the particle physics setup followed by the details of DM and majoron cosmology in section III. In section IV, and section V respectively, we discuss the details of DM decay and domain wall disappearance emitting gravitational waves due to QG scale suppressed operators. We finally conclude in section VI.

II. THE SETUP

The relevant field content and respective transformations under $SU(2)_L \times U(1)_Y \times U(1)_L$ symmetry are shown in table I with the BSM fields being the right handed neutrino N_R , fermion DM χ and the singlet scalar Φ responsible for spontaneous symmetry breaking. While the specific choice of Q_L , the lepton number charge of χ_L does not affect our conclusion, we consider $Q_L \neq -1$, such that DM remains stable at renormalisable level. The relevant part of the Yukawa Lagrangian can be written as

$$-\mathcal{L}_Y \supset \frac{f_i}{2} \Phi \overline{N_{Ri}^c} N_{Ri} + Y_{\alpha i} \overline{\ell_{L\alpha}} \tilde{H} N_{Ri} + y_\chi \overline{\chi_L} \Phi \chi_R + \text{h.c.} \quad (1)$$

The scalar potential is

$$V(H, \Phi) = \lambda_H \left(H^\dagger H - \frac{v^2}{2} \right)^2 + \lambda_\Phi \left(|\Phi|^2 - \frac{v_\Phi^2}{2} \right)^2 + \lambda_{H\Phi} \left(H^\dagger H - \frac{v^2}{2} \right) \left(|\Phi|^2 - \frac{v_\Phi^2}{2} \right) \quad (2)$$

where $v(v_\Phi)$ denotes the VEV of $H(\Phi)$. The spontaneous breaking of $U(1)_L$ global symmetry after Φ acquires a VEV, leads to a massless Goldstone boson or majoron, identified as the angular part of the field Φ . A non-zero majoron mass can be generated via explicit $U(1)_L$ breaking terms of the form

$$V_L = -\frac{m^2}{4}(\Phi^2 + \text{h.c.}) \quad (3)$$

which breaks $U(1)_L$ to a remnant Z_2 symmetry in the scalar potential. It should be noted that we have considered the simplest form of explicit $U(1)_L$ breaking to generate the mass of majoron. Other forms of explicit $U(1)_L$ breaking will lead to different remnant symmetry. For example, explicit $U(1)_L$ breaking terms like Φ^3, Φ^4 will correspond to remnant symmetry Z_3, Z_4 respectively. Allowing, the explicit breaking to occur via non-renormalisable operators Φ^n/Λ^{n-4} will lead to bigger remnant symmetry groups like Z_n where $n > 4$. The details of the domain wall formation, evolution and emission of GW differs from the simplest Z_2 domain walls discussed in this work. Phenomenology of such Z_n ($n > 2$) domain walls can be found in [49–51] and references therein.

After the spontaneous breaking of global $U(1)_L$ symmetry, we can represent $\Phi = (v_\Phi + \phi + i\eta)/\sqrt{2}$, where η denotes the majoron. From the potential terms in Eq. (2) and Eq. (3), the masses of Higgs (h), ϕ and majoron can be written as [52, 53]

$$m_h^2 \simeq 2\lambda_H v^2, \quad m_\phi^2 = 2\lambda_\Phi v_\Phi^2, \quad m_\eta^2 \simeq m^2. \quad (4)$$

The coupling between the majoron and heavy right-handed neutrino can be written as

$$-\mathcal{L} \supset \frac{if_i}{2\sqrt{2}}\eta\bar{N}_i\gamma^5 N_i = \frac{im_{N_i}}{2v_\Phi}\eta\bar{N}_i\gamma^5 N_i. \quad (5)$$

Similarly, the coupling between the majoron and DM can be written as

$$-\mathcal{L} \supset \frac{iy_\chi}{\sqrt{2}}\eta\bar{\chi}\gamma^5 \chi = \frac{im_\chi}{v_\Phi}\eta\bar{\chi}\gamma^5 \chi. \quad (6)$$

The details of derivation of coupling between CP-odd and CP-even scalars with $N_i = N_{R_i} + N_{R_i}^c$ and $\chi = \chi_L + \chi_R$ are given in appendix A. Light neutrino mass arises from the type-I seesaw mechanism as

$$m_\nu = -M_D m_N^{-1} M_D^T \quad (7)$$

where $M_D = Yv/\sqrt{2}$ is the Dirac mass. Here $m_{N_i} = f_i v_\Phi/\sqrt{2}$, $m_\phi = \sqrt{2\lambda_\Phi} v_\Phi$, $m_\chi = y_\chi v_\Phi/\sqrt{2}$. The free parameters of the model, relevant for the phenomenology, are

$f_i, Y_{\alpha i}, y_\chi, v_\Phi, \lambda_\Phi, \lambda_{H\Phi}$ and m_η . In terms of masses of RHNs, ϕ and χ , the free parameters are $m_{N_i}, m_\chi, m_\phi, v_\Phi, Y_{\alpha i}, \lambda_{H\Phi}$ and m_η . We also denote the RHNs simply as N hereafter.

Finally, there exists no exact (continuous or discrete) global symmetry in the theory of QG [54]. In other words, any global symmetry of a given effective field theory (EFT) is at best an approximate symmetry emergent in the IR [55] and should be broken by a higher-dimensional operator. As a result, the remnant Z_2 present in this setup will also be explicitly broken by the higher dimensional operators [56]³,

$$\Delta V = \frac{1}{\Lambda_{\text{QG}}}(\alpha_1 \Phi^5 + \alpha_2 \Phi^3 H^2 + \alpha_3 \Phi H^4), \quad (8)$$

where Λ_{QG} denotes the scale of QG. Here we assume a common origin and therefore a common scale for the breaking of all global symmetries, and for simplicity, we take all the dimensionless coefficients in Eq. (8) to be of the same order, and we can make them of $\mathcal{O}(1)$ by redefining Λ_{QG} .

III. COSMOLOGY OF MAJORON AND DARK MATTER

Majoron can have very interesting cosmology with the details being dependent upon its mass and interactions. Very light majorons in eV or sub-eV scale with negligible interactions can be approximated as a coherently oscillating scalar field, produced via the misalignment mechanism similar to axions [58–61]. Depending upon the initial displacement or kinetic energy of the scalar field, majoron can play the role of cold dark matter in the Universe. In addition to that, majoron can also lead to spontaneous baryogenesis via leptogenesis [62–77]. In this work, we neither consider majoron DM nor spontaneous leptogenesis. This allows more available parameter space in singlet majoron model which otherwise gets constrained when majoron plays the role of DM [78, 79]. Also, majoron DM is not perfectly stable but long-lived. However, one of our motivations is to study the effect of QG scale on lifetime of DM, which otherwise is perfectly stabilised by a global symmetry. Also considering thermal leptogenesis from RHN decay makes the scenario independent of any initial conditions. While leptogenesis can occur from CP violating out-of-equilibrium decays of right handed

³ See [57] and references therein for similar discussions in QCD axion models with Peccei-Quinn $U(1)$ global symmetry.

neutrinos in type-I seesaw, DM is in the form a separate fermion field which couples to the SM via radial and angular mode (majoron) of the singlet scalar field responsible for spontaneous breaking of global lepton number symmetry. We consider sizeable coupling of majoron with the SM bath such that it can be thermally produced. Such majorons can not only act like a portal between DM and SM but can also contribute to the effective relativistic degrees of freedom, observable at cosmic microwave background (CMB) experiments. Heavy majorons above the eV scale, which do not contribute to DM, are likely to decay into the SM particles without leaving any relic in the present Universe.

We first discuss the thermalisation of majoron, η . For this, we have considered the scattering process, $N\eta \rightarrow N\eta$ and compare its rate with the Hubble expansion rate of the Universe \mathcal{H} . In the left panel plot of Fig. 1, we show the ratio of interaction rate ($\Gamma = n_N^{\text{eq}} \langle \sigma v \rangle_{N\eta \rightarrow N\eta}$) to \mathcal{H} as a function of temperature for three different values of v_Φ . For a larger m_N/v_Φ ratio (in other words, a larger f), we can have thermalised majoron. It is found that as long as $m_\eta \ll m_N$, the thermalisation of majoron is independent of its mass. In the right panel plot of Fig. 1, we show the parameter space in m_N vs v_Φ plane where majoron thermalises. We have not considered the upper triangular region where $m_N > v_\Phi$, where the coupling can become non-perturbative.

Light majoron in sub-eV ballpark can contribute to the effective relativistic degrees of freedom ΔN_{eff} tightly constrained by CMB observations as well as successful big bang nucleosynthesis (BBN). Majoron contribution to ΔN_{eff} can be calculated based on the thermal history of majoron. The contribution to ΔN_{eff} from light thermal majoron at the epoch of recombination is given as

$$\Delta N_{\text{eff}} \equiv \frac{\rho_\eta(T_{\text{CMB}})}{\rho_{\nu,1}(T_{\text{CMB}})} = 0.027 \times \left(\frac{106.75}{g_*(T_{\text{dec}})} \right)^{4/3}. \quad (9)$$

Here ρ_η and $\rho_{\nu,1}$ denotes the energy density of majoron and a single species of active neutrino respectively and g_* denotes the effective degrees of freedom of SM particles. For all the blue shaded region shown in the right panel plot of Fig. 1, majoron gets decoupled at a temperature larger than 100 GeV. This gives a constant contribution of thermal majoron $\Delta N_{\text{eff}} = 0.027$ for all v_Φ . Future CMB experiment, specially, CMB-HD [80] can probe ΔN_{eff} upto 0.014 at 1σ , keeping thermalised light majoron parameter space verifiable. We also check the non-thermal production of majorons from topological defects like cosmic strings and domain walls in our model [81] and find the corresponding abundance to be

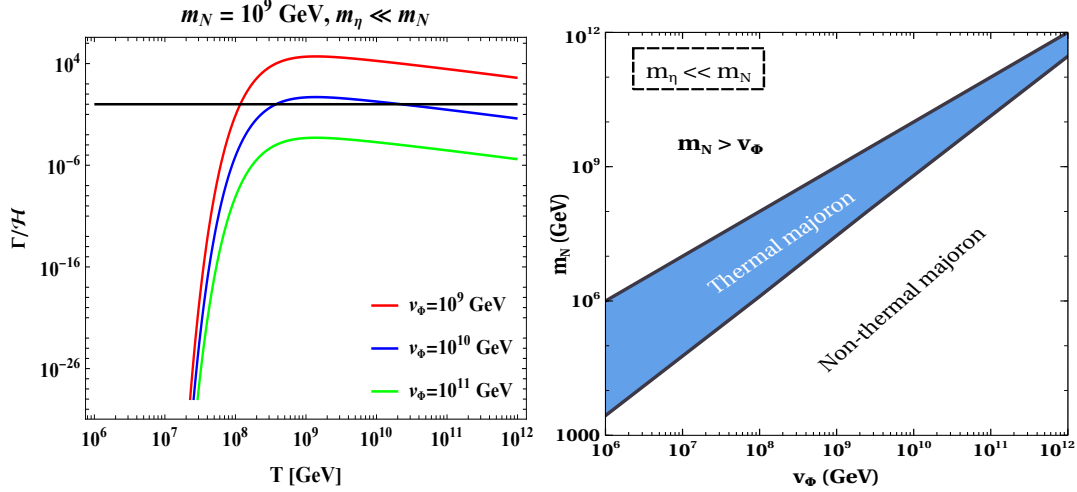


FIG. 1: Left panel: majoron interaction rate in comparison to the Hubble expansion rate. Right panel: Parameter space in RHN mass m_N and singlet scalar VEV v_Φ showing the thermalisation region of majoron for $m_\eta \ll m_N$.

sub-dominant compared to DM, for the region of parameter space considered in our work.

DM couples to the SM bath or RHNs only via ϕ, η with a coupling proportional to m_χ/v_Φ . We consider $v_\Phi \geq 10^6$ GeV motivated from type-I seesaw, leptogenesis as well as domain wall related gravitational wave signatures to be discussed below. For such a high scale symmetry breaking, DM can not have large sizeable portal couplings required for thermal freeze-out, for typical thermal DM masses around the electroweak scale, below the unitarity limit [82]. Therefore, it is more natural to consider freeze-in dark matter [83]. Depending upon the mass spectrum of newly introduced particles, here we discuss two different scenarios for freeze-in DM.

A. Dark matter with $m_\phi > 2m_N$

To begin with, we consider the mass spectrum as $m_\phi > 2m_N > m_\chi > m_\eta$. We assume that RHNs are in thermal bath via the Yukawa interaction with SM leptons and Higgs. Similarly, ϕ is taken to be in thermal equilibrium initially. The DM is considered to be feebly interacting, produced through two possible ways : from decay of CP even scalar ($\phi \rightarrow \chi\bar{\chi}$) and from annihilation of RHNs ($N\bar{N} \rightarrow \chi\bar{\chi}$ with η and ϕ as the mediator). Assuming N to be in thermal equilibrium, the Boltzmann equations (BE) for ϕ and χ can

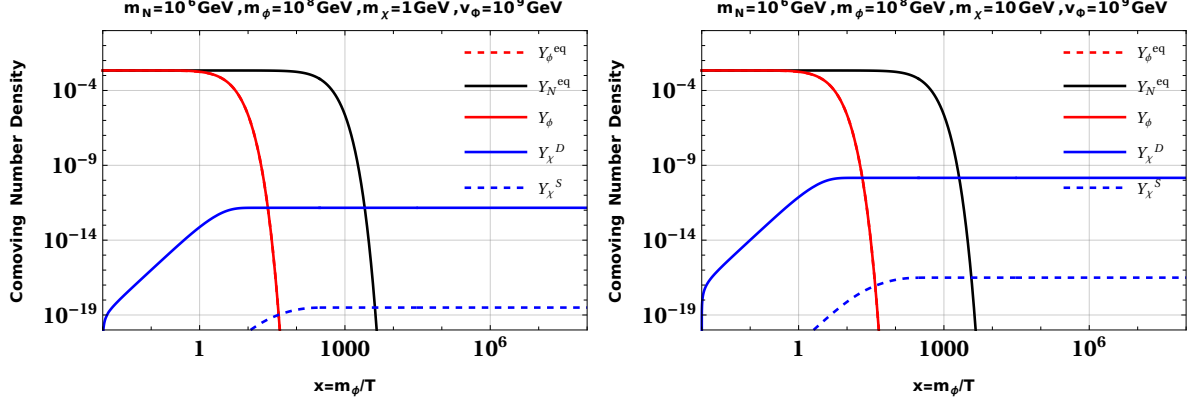


FIG. 2: Evolution plot for $m_\phi > 2m_N$ for two different $m_\chi = 1$ GeV (left panel) and $m_\chi = 10$ GeV (right panel). Due to the inverse decay of N , ϕ follows equilibrium abundance throughout its lifetime. The blue solid and dashed lines represent the respective contributions to DM production from the decay of ϕ and the annihilation of N .

be written as

$$\frac{dY_\phi}{dx} = -\frac{\beta s}{\mathcal{H}x} \langle \sigma v \rangle_{\phi\phi \rightarrow N\bar{N}} (Y_\phi^2 - (Y_\phi^{\text{eq}})^2) - \frac{\beta}{\mathcal{H}x} \Gamma_{\phi \rightarrow N\bar{N}} \frac{K_1(m_\phi/T)}{K_2(m_\phi/T)} (Y_\phi - Y_\phi^{\text{eq}}) \quad (10)$$

$$-\frac{\beta}{\mathcal{H}x} \Gamma_{\phi \rightarrow \chi\bar{\chi}} \frac{K_1(m_\phi/T)}{K_2(m_\phi/T)} Y_\phi, \quad (11)$$

$$\frac{dY_\chi}{dx} = \frac{\beta}{\mathcal{H}x} \Gamma_{\phi \rightarrow \chi\bar{\chi}} \frac{K_1(m_\phi/T)}{K_2(m_\phi/T)} Y_\phi + \frac{\beta s}{\mathcal{H}x} \langle \sigma v \rangle_{N\bar{N} \rightarrow \chi\bar{\chi}} (Y_N^{\text{eq}})^2.$$

Here, Y and s represent the comoving number density and entropy density respectively. The effect due to change of $g_{*,s}$ is incorporated into the parameter $\beta = \left[1 + \frac{T dg_{*,s}/dT}{3g_{*,s}}\right]$ and $x = m_0/T$ where m_0 is some arbitrary reference mass. We consider $m_0 = m_\phi$ for numerical calculations. K_i 's denote modified Bessel functions of the second kind whereas \mathcal{H} denotes the Hubble expansion rate. The expression for relevant cross-sections are given in appendix B.

In Fig. 2, the evolution of N , ϕ and χ are shown. Here Y_χ^D and Y_χ^S denote the contribution to the DM production from the 1st and 2nd terms respectively in the BE for Y_χ . Due to the inverse decay and annihilation of N , ϕ remains in equilibrium during its evolution. Also, the production of DM from annihilation is subdominant compared to the production from decay of ϕ , as expected. Increasing DM mass from left to the right panel plots increases both Y_χ^D and Y_χ^S as both $\Gamma_{\phi \rightarrow \chi\bar{\chi}}$ and $\langle \sigma v \rangle_{N\bar{N} \rightarrow \chi\bar{\chi}}$ are proportional to m_χ^2 .

Fig. 3 shows the parameter space in v_ϕ vs m_N plane with DM relic satisfying regions are

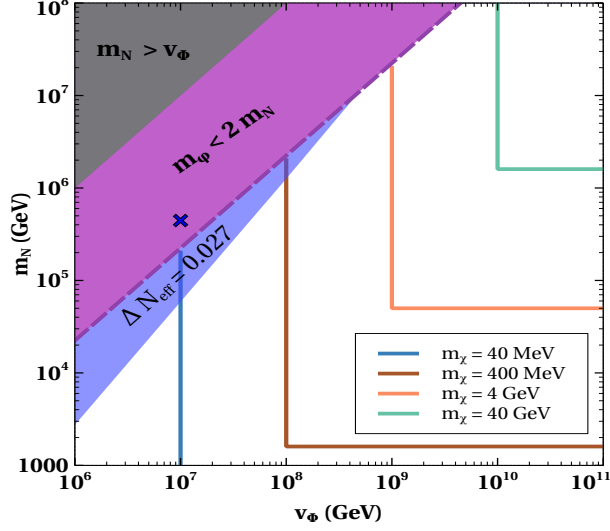


FIG. 3: Parameter space in v_ϕ vs m_N plane with different colored contours denoting relic satisfying regions for different DM masses.

shown as colored contours for different DM masses. Here, λ_ϕ is taken as 10^{-3} . This fixes m_ϕ for a given v_ϕ . In the gray and magenta region $m_N > v_\phi$ and $m_\phi < 2m_N$ respectively. The dashed magenta color line denotes $m_\phi = 2m_N$. As depicted in the evolution plots of Fig. 2, the production of dark matter from decay of ϕ dominates over the production from annihilation across the entire parameter space. The four different colored contours correspond to different DM masses that satisfy correct relic abundance. Staring from the dashed magenta line, a change in m_N does not change the DM relic for fixed v_ϕ and m_χ . This is because, in the vertical portion, the coupling between N and ϕ (which is $\propto \frac{m_N}{v_\phi}$) is larger enough so that ϕ remains in equilibrium due to the inverse decay of N ($N\bar{N} \rightarrow \phi$). However the situation reverses for a sufficiently small values of m_N where ϕ does not always follow the equilibrium distribution. In that region, a different v_ϕ (as well as m_ϕ), does not alter DM abundances. Hence, the horizontal portion of the curves are obtained. Moreover, to indicate the parameter space that comes within the sensitivities of future CMB-HD experiment, we show the blue colored region where majoron thermalises (from Fig. 1).

B. Dark matter with $m_\phi < 2m_N$

For the mass spectrum $2m_N > m_\phi > m_\chi > m_\eta$, i.e. the magenta shaded region in Fig. 3, the decay of $\phi \rightarrow N\bar{N}$ ceases. Hence we have only the 1st and last term in the right hand

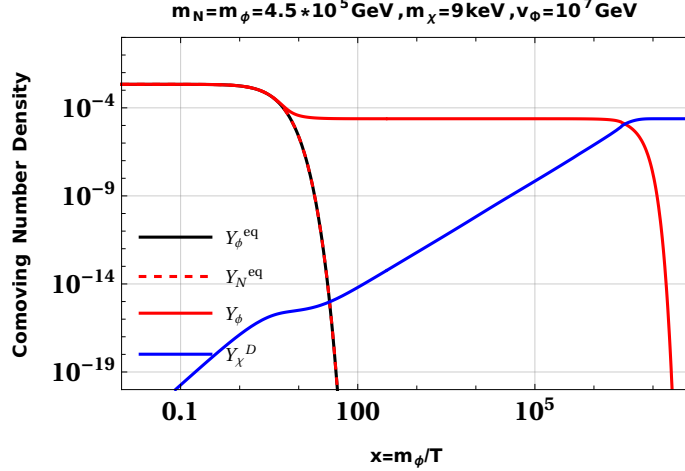


FIG. 4: Evolution plot for $m_\phi < 2m_N$. Here, we take $m_N = m_\phi$. The contribution from the $N\bar{N} \rightarrow \eta\eta$ is negligible, hence not shown here.

side of equation (10). Due to the presence of only one decay channel of ϕ , the comoving DM abundance get enhanced. To see it, we consider a point in Fig. 3 denoted by \times . The evolution plot for this point is shown in Fig. 4. In the plot, $v_\Phi = 10^7$ GeV and $\lambda_\Phi = 10^{-3}$. This gives $m_\phi = 4.5 \times 10^5$ GeV. Mass of N is taken to be equal to m_ϕ . As shown in the plot, for these choice of parameters a higher comoving abundance is obtained requiring DM mass to be as low as 9 keV for correct relic density. Also due to such low DM mass, the decay width of ϕ is small ($\propto m_\chi^2$) resulting ϕ decaying very close to the BBN era. This brings two major problems namely, (i) the late decay of ϕ leads to a large the free-streaming length of DM (as shown in [84, 85]) potentially giving hot DM that is already ruled out from structure formation constraint; (ii) DM mass range lies in the boundary of Tremaine-Gunn bound for fermionic dark matter [86]. These problems get worse for a higher v_Φ making the scenario $m_\phi < 2m_N$ for $\lambda_\phi = 10^{-3}$ disfavoured. Hence, for our current and future DM analysis, we only consider the region below the dashed magenta line in Fig. 3.

C. Leptogenesis

Apart from producing correct relic abundance, the current set up also allows to explain the observed baryon asymmetry of the Universe via thermal leptogenesis. The CP violating out-of-equilibrium decay of RHN neutrinos produce lepton asymmetry which is later converted to baryon asymmetry by SM sphalerons. Assuming hierarchical RHN mass spectrum, the

baryon-to-photon ratio can be estimated as

$$\eta_B \simeq 10^{-2} \epsilon_1 \kappa_1, \quad (12)$$

where ϵ_1 denotes the CP asymmetry and κ_1 represents the efficiency factor. We use the maximum value of CP asymmetry parameter which is given as

$$|\epsilon_1| \leq \frac{3m_{N_1} \sqrt{(\Delta m_{\text{atm}})^2}}{8\pi v^2}. \quad (13)$$

Here $(\Delta m_{\text{atm}})^2 \simeq 2.4 \times 10^{-3} \text{eV}^2$ denotes the active neutrino atmospheric mass-squared difference. We consider efficiency factor to be 0.01 that corresponds to strong wash-out regime. Apart from usual leptogenesis in type-I seesaw, in this setup we have extra annihilation channel, $N\bar{N} \rightarrow \eta\eta$ that can keep RHNs in equilibrium for longer and hence dilute the final baryon asymmetry. However for strong washout regime and for equilibrium initial abundance of N , the effect from $N\bar{N} \rightarrow \eta\eta$ can be neglected. With this, using Eq. (12), we get that the mass of RHN should be larger than $m_{N_1} \gtrsim 6 \times 10^{10} \text{ GeV}$. Imposing the condition of correct DM abundance along with correct baryon asymmetry, one needs $m_\phi > 2m_N \implies v_\phi > \frac{2m_N}{\sqrt{2\lambda_\Phi}}$. To make the calculations consistent with the DM and GW analysis, we consider $\lambda_\Phi = 10^{-3}$ which gives v_ϕ larger than $\sim 3 \times 10^{12} \text{ GeV}$. Such large values of v_ϕ are disfavoured from DW overclosure and DM properties, as we discuss below. With the help of flavor leptogenesis, the minimum m_{N_1} can be relaxed upto one order of magnitude [87, 88] than the value obtained from Eq. (12). Hence the corresponding value of v_ϕ can also be reduced upto one order magnitude. For a even smaller value of v_ϕ , required amount of lepton asymmetry can be created via resonant leptogenesis [89]. Resonant leptogenesis can enhance CP asymmetry parameter upto $\mathcal{O}(0.1)$ where two RHNs have nearly the same mass, with the mass splitting being nearly equal to the its decay width. Therefore, correct baryon asymmetry is possible via resonant scenario where v_ϕ is as small as 10^6 GeV .

IV. DARK MATTER DECAY VIA QUANTUM GRAVITY EFFECTS

In the present setup, the QG effects also break the $U(1)_L$ symmetry explicitly, and as a result, the DM decay can occur via dimension five operators of the type

$$-\mathcal{L}_{\text{decay}} \supset \frac{Y_{D_\alpha}}{\Lambda_{\text{QG}}} \bar{\ell}_{L\alpha} \tilde{H} \chi_R \Phi + \text{h.c.}, \quad (14)$$

where $\tilde{H} = i\sigma_2 H^*$. As discussed earlier, we assume that all the global symmetries are broken by a common scale i.e. we simply consider all the dimensionless coefficients in Eq. (8) and Eq. (30) to be of the same order, and we set them to be $\mathcal{O}(1)$ by redefining Λ_{QG} . Looking at Eq. (30), one notices that, once the electroweak symmetry is broken, the DM χ mixes with the SM neutrinos with a mixing angle [35, 90],

$$\theta \simeq \sum_{\alpha=1,2,3} \left(\frac{Y_{D_\alpha} v_\Phi v}{\sqrt{2} \Lambda_{\text{QG}} m_\chi} \right). \quad (15)$$

As a result of this mixing, the DM decays to the SM particles. This provides us a possibility to look for dark matter in the indirect search experiments. Once such example is constraining the DM decay life time by the detection of the galactic and extra-galactic diffuse X/ γ -ray background. Due to the mixing, the DM can have two-body (one-loop level mediated via W^\pm and SM charged leptons) and three-body (at tree-level mediated via W^\pm) decay channels that can dominate if kinematically allowed. At one-loop level χ can decay to photons and active neutrinos via $\chi \rightarrow \nu\gamma$, the decay rate of which is given by [91, 92]

$$\begin{aligned} \tau_{\chi \rightarrow \nu\gamma} &\simeq \left(\frac{9\alpha_{\text{EM}} \sin^2 \theta}{1024\pi^4} G_F^2 m_\chi^5 \right)^{-1} \\ &\simeq 1.8 \times 10^{17} \text{ s} \left(\frac{10 \text{ MeV}}{m_\chi} \right)^5 \left(\frac{\sin \theta}{10^{-8}} \right)^{-2}, \end{aligned} \quad (16)$$

with $\alpha_{\text{EM}} = 1/137$ being the electromagnetic fine-structure constant and G_F denoting the Fermi constant. The three-body decay channel $\chi \rightarrow e^+e^-\nu$, the decay rate of which can be approximately expressed as [92, 93]

$$\begin{aligned} \tau_{\chi \rightarrow e^+e^-\nu} &\simeq \left(\frac{c_\alpha \sin^2 \theta}{96\pi^3} G_F^2 m_\chi^5 \right)^{-1} \\ &\simeq 2.4 \times 10^{15} \text{ s} \left(\frac{10 \text{ MeV}}{m_\chi} \right)^5 \left(\frac{\sin \theta}{10^{-8}} \right)^{-2}, \end{aligned} \quad (17)$$

where $c_\alpha = (1 + 4\sin^2 \theta_W + 8\sin^4 \theta_W)/4 \simeq 0.59$ with θ_W being the weak mixing angle. Contributions from the above two channels to the X/ γ -ray fluxes are roughly at similar levels [92]. The null detection of X-rays and γ -rays line sets a lower bound on the lifetime of the decaying DM that can further be converted into the constraints on the the DM mass and the mixing angle. The observed diffuse photon spectra data obtained from the HEAO-1 [94], INTEGRAL [95], COMPTEL [96] and EGRET [97] satellites can restrict the parameter space of m_χ and θ within the range $0.01 \text{ MeV} \lesssim m_\chi \lesssim 100 \text{ MeV}$, which can be

parameterized as $\theta^2 \lesssim 2.8 \times 10^{-18} (\text{MeV}/m_\chi)^5$ [98]. With the help of the expression of θ in Eq. (15), we have

$$\left(\frac{3v_\Phi v}{\sqrt{2}\Lambda_{\text{QG}}m_\chi} \right)^2 \lesssim 2.8 \times 10^{-18} \left(\frac{\text{MeV}}{m_\chi} \right)^5, \quad (18)$$

where we consider that the DM interacts with different generations of neutrinos with the identical $\mathcal{O}(1)$ strength. On top of this, the Fermi Large Area Telescope (Fermi-LAT) [99, 100] has presented a dedicated line search of the diffuse γ -ray background, the null result of which also constrains the lifetime of the DM within the mass range $1 \text{ GeV} \lesssim m_\chi \lesssim 1 \text{ TeV}$. Here we take the 95% C.L. limit on the lifetime of decaying DM given by ref. [101], which assumes a Navarro-Frenk-White (NFW) profile for the DM distribution [102].

DM decay also faces stringent constraints from CMB, if the decay occurs after or during the recombination. The DM decay can re-ionize the intergalactic medium, and hence can modify the CMB power spectrum. Accurate measurements of the CMB spectrum have been implemented by recent experiments including WMAP [103], ACT [104], SPT [105] and Planck [2]. The 95% C.L. lower bounds on the DM decay lifetime have been given in ref. [106], showing that $\tau_{\text{DM}} \gtrsim 10^{25} \text{ s}$ for decays into both e^+e^- pairs and photons. These DM decays can also introduce radio signals originating inside the DM-dominated galaxies and clusters, if the produced e^+e^- pairs undergo energy loss via electromagnetic interactions in the interstellar medium. Such radio waves can be tested by radio telescopes like the Square Kilometer Array (SKA) radio telescope [107]. It is found that the DM decay width up to $\Gamma_{\text{DM}} \gtrsim 10^{-30} \text{ s}^{-1}$ is detectable at SKA assuming 100-hour observation time [108]. We will incorporate these constraints while showing the final allowed parameter space, to be discussed below.

V. DOMAIN WALLS AND GRAVITATIONAL WAVES

Domain walls, a cosmological catastrophe, are 2-dimensional topological defects resulting from a spontaneous symmetry breaking (SSB) of a discrete symmetry like Z_2 , as also considered in the present setup. Once formed, their energy density varies inversely with the scale factor (a^{-1}) which is much slower than that of matter (a^{-3}) or radiation (a^{-4}). As a result, they can dominate the energy budget of the Universe at some later stage and can alter the fate of CMB observations or successful light nuclei synthesis during BBN. These cosmological catastrophes can be avoided by introducing an energy bias in the scalar po-

tential that makes the vacuum unstable. The above scaling of the DW is true assuming the radiation-dominated era when the DWs were relativistic. At a later stage, the DW dynamic is dominated by its tension force that stretches the DWs up to the horizon size. Numerical studies [109–113] have shown that the evolution of DW in this regime can be described by the scaling solution. Here, their energy density evolves according to the simple scaling law $\rho_{\text{DW}} \propto t^{-1}$ where ρ_{DW} denotes the energy density of the DW and their typical size is given by Hubble radius $\sim t^2$. In the scaling regime, their energy density can be expressed as,

$$\rho_{\text{DW}} = \sigma \frac{\mathcal{A}}{t}, \quad (19)$$

with $\mathcal{A} \simeq 0.8$ being the area parameter [114] and σ being the surface tension of the DW. In the present setup this can be achieved with the help of QG effect as it is expected to break any global symmetry at high scale. Following this, one can write the energy bias after replacing fields with their VEVs, this leads to a bias contribution to the effective potential of the form

$$V_{\text{bias}} \simeq \frac{1}{\Lambda_{\text{QG}}} \left(v_{\Phi}^5 + \frac{v_{\Phi}^3 v^2}{2} + \frac{v_{\Phi} v^4}{4} \right). \quad (20)$$

Due to this uplifting of degeneracy, the DW starts to collapse and annihilate, resulting in the production of SGWB whose signals can be tested in the present and future GW detectors. Under the assumption that $v_{\Phi} \gg v$, a sufficiently large V_{bias} can be achieved rendering the production of observable GW signals. Note that to have a DW, a very large V_{bias} must be avoided according to the prediction of percolation theory [29]. Under such a hierarchy, the bias potential is dominated by,

$$V_{\text{bias}} \simeq \frac{v_{\Phi}^5}{\Lambda_{\text{QG}}}. \quad (21)$$

Before delving into the details of GW production from the annihilation of the DW, we first like to discuss the constraints that appear on the V_{bias} as a result of DW annihilations to the SM particles. If the energy bias of the DW is very small, they live for a very long time ($t_{\text{ann}} \propto \frac{1}{V_{\text{bias}}}$, with t_{ann} being the annihilation time of the DW). Requiring that their collapse happens before they dominate the energy budget of the Universe puts a lower bound on the magnitude of V_{bias} [29],

$$V_{\text{bias}}^{1/4} > 2.18 \times 10^{-5} \text{GeV} C_{\text{ann}}^{1/4} \mathcal{A}^{1/2} \left(\frac{\sigma^{1/3}}{10^3 \text{GeV}} \right)^{3/2}, \quad (22)$$

where $C_{\text{ann}} \simeq 2$ is a dimensionless constant, and $\sigma = \sqrt{\frac{8\lambda_\Phi}{9}} v_\Phi^3$ is the surface tension of the DW. Even if Eq. (22) is satisfied and the DW are annihilated away before their dominance, their decay products (assuming they are the SM particles) can still destroy the light elements created at BBN epoch. This demands $t_{\text{ann}} \leq 0.01$ s and hence an additional constraint on the magnitude of the energy bias can be obtained as,

$$V_{\text{bias}}^{1/4} > 5.07 \times 10^{-4} \text{GeV} C_{\text{ann}}^{1/4} \mathcal{A}^{1/4} \left(\frac{\sigma^{1/3}}{10^3 \text{GeV}} \right)^{3/4}. \quad (23)$$

The production of the GW from DW annihilation has been investigated in detail, for example, see refs. [29–31, 46, 114–117]. Assuming that the DW annihilate instantaneously ($t = t_{\text{ann}}$) during the radiation-dominated era, the peak frequency f_p and peak energy density spectrum $\Omega_p h^2$ of GW at present can be expressed as [29, 118]

$$\begin{aligned} f_p &\simeq 3.75 \times 10^{-9} \text{ Hz} \times C_{\text{ann}}^{-1/2} \mathcal{A}^{-1/2} \left(\frac{10^3 \text{ GeV}}{\sigma^{1/3}} \right)^{3/2} \left(\frac{V_{\text{bias}}^{1/4}}{10^{-3} \text{ GeV}} \right)^2, \\ \Omega_p h^2 &\simeq 5.3 \times 10^{-20} \times \tilde{\epsilon}_{\text{GW}} C_{\text{ann}}^2 \mathcal{A}^4 \left(\frac{\sigma^{1/3}}{10^3 \text{ GeV}} \right)^{12} \left(\frac{10^{-3} \text{ GeV}}{V_{\text{bias}}^{1/4}} \right)^8, \end{aligned} \quad (24)$$

where $\tilde{\epsilon}_{\text{GW}} \simeq 0.7$ [114] denotes the fraction of energy radiated into GW and can be regarded as a constant in the scaling regime. The typical feature of the GW spectrum from DW is that it follows a broken power law, where the breaking point has a frequency determined by the annihilation time and the peak amplitude is determined by the energy density in the domain walls as can be seen from Eq. (24). To depict the GW spectrum, we adopt the following parametrization for a broken power-law spectrum [119, 120]

$$\Omega_{\text{GW}} h^2 = \Omega_p h^2 \frac{(a+b)^c}{(bx^{-a/c} + ax^{b/c})^c}, \quad (25)$$

where $x \equiv f/f_p$, and a , b and c are real and positive parameters. Here the low-frequency slope $a = 3$ can be fixed by causality, while numerical simulations suggest $b \simeq c \simeq 1$ [114].

Apart from the constraint on DW from equations (22) and (23), a large amplitude of GW from DW annihilation can also contribute to extra effective number of relativistic species, ΔN_{eff} . This gives an upper bound on the GW energy density. Considering the Planck 2018 results on ΔN_{eff} at the time of BBN, the constraint on GW energy density is given as [121]

$$\Omega_{\text{GW,BBN}} < \frac{7}{8} \left(\frac{4}{11} \right)^{4/3} \Delta N_{\text{eff}} \sim 0.05. \quad (26)$$

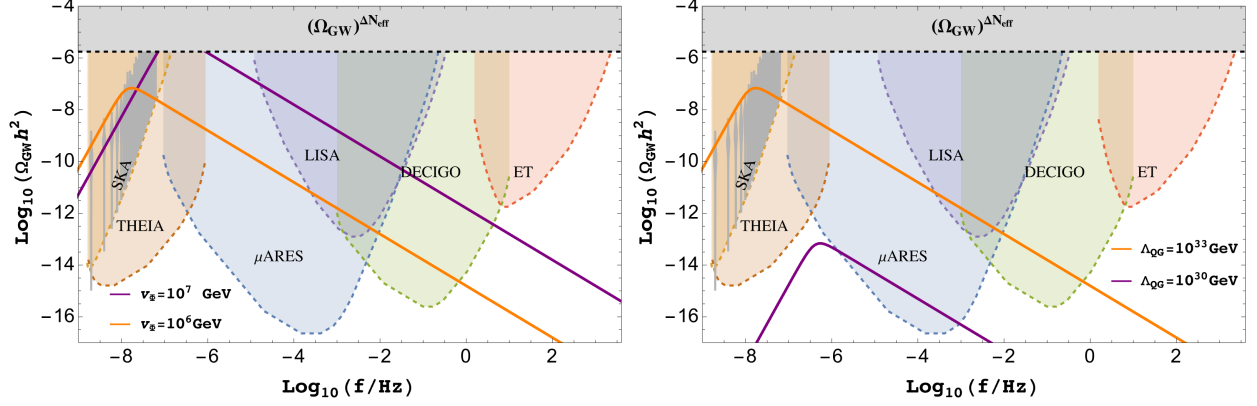


FIG. 5: The orange and purple curve show the GW spectrum generated from the annihilation of the DW. In both the panels, we set $\lambda_\Phi = 10^{-3}$ just for the demonstrative purpose. While in the left Panel we fix $\Lambda_{\text{QG}} = 10^{33}$ GeV and vary v_Φ , in the right panel we fix $v_\Phi = 10^6$ GeV and vary Λ_{QG} . The gray color region denotes the portion excluded from ΔN_{eff} bound.

Hence, the maximum energy density of GW today which is allowed from ΔN_{eff} bound can be written as

$$\Omega_{\text{GW}}^{\Delta N_{\text{eff}}} h^2 = 0.39 \left(\frac{g_*(T_{\text{BBN}})}{106.75} \right)^{-1/3} \Omega_{r,0} h^2 \Omega_{\text{GW,BBN}} \simeq 1.75 \times 10^{-6}, \quad (27)$$

where $\Omega_{r,0} h^2 \sim 4.18 \times 10^{-5}$ represents current radiation energy density fraction. Therefore, to be consistent with this bound, the peak energy density of GW from DW, $\Omega_p h^2$, should be less than $\Omega_{\text{GW}}^{\Delta N_{\text{eff}}} h^2$.

In Fig. 5, we present the GW spectrum for different choices of model parameters. For both the plots we set $\lambda_\Phi = 10^{-3}$. In Fig. 5, the gray violins indicate the GW spectrum observed by the NANOGrav. We notice that the spectra shown by the orange color lines in the Fig. 5 are in good agreement with the NANOGrav 15-year result. Such domain wall interpretation of the NANOGrav 15-year data was also discussed in earlier works, see [27] and references therein. Using Eq. (25), we also evaluate the sensitivity curves of the future GW detectors ET [122], LISA [123], DECIGO [124], μAres [125], SKA [126], IPTA [127] and THEIA [128] by calculating the signal-to-noise ratio (SNR) [129, 130]

$$\varrho = \left[n_{\text{det}} t_{\text{obs}} \int_{f_{\text{min}}}^{f_{\text{max}}} df \left(\frac{\Omega_{\text{signal}}(f)}{\Omega_{\text{noise}}(f)} \right)^2 \right]^{1/2}, \quad (28)$$

where $n_{\text{det}} = 1$ for auto-correlated detectors and $n_{\text{det}} = 2$ for cross-correlated detectors, t_{obs} denotes the observational time, and Ω_{noise} represents the noise spectrum expressed in terms

of the GW energy density spectrum [131]. Integrating $(\Omega_{\text{signal}}/\Omega_{\text{noise}})^2$ over the sensitive frequency range of individual GW detectors, we obtain the SNRs for the GW spectra. Now, in the left panel, we fix the QG scale at $\Lambda_{\text{QG}} = 10^{33}$ GeV while we vary v_Φ . Following Eq. (24), one finds that for dimension 5 operator, $\Omega_p h^2 \propto (\lambda_\Phi^2 \Lambda_{\text{QG}}^2)/v_\Phi^2$ while $f_p \propto v_\Phi/(\lambda_\Phi^{1/4} \Lambda_{\text{QG}}^{1/2})$. As expected, a larger v_Φ results in a smaller $\Omega_p h^2$ and a larger peak frequency. On the other hand, a larger Λ_{QG} scale corresponds to a larger $\Omega_p h^2$ but a smaller peak frequency, this behavior is visible in the right panel of Fig. 5.

BPs	Λ_{QG} (GeV)	v_Φ (GeV)	m_N (GeV)	m_χ (MeV)	ΔN_{eff}
BP1	10^{33}	10^7	10^5	40	0.027
BP2	10^{33}	10^6	10^4	4	0.027

TABLE II: Set of benchmark values of Λ_{QG} and v_Φ .

In Fig. 6, we summarise our result. For the demonstrative purpose, we consider different benchmark points (BPs) shown in Table II. While in the left panel, we show BP1, in the right panel, we show BP2. In both plots, the light gray and the yellow-shaded regions are excluded from the null detection of X-ray signals originating from the DM decay and CMB observations respectively, as discussed in the previous section. The black dashed lines label the testing capabilities of the upcoming SKA telescope. The pink and gray-shaded regions are excluded from the constraints coming from the DW overclosure and BBN. The BBN limit arises from the requirement of not disrupting light nuclei abundance from DW annihilations at late epochs. We would also like to point out that the ΔN_{eff} bounds on the GW is much weaker than the one obtained from the DW overclosure and hence we do not show it in the plots. The parameter space below the horizontal dot-dashed line remains within the sensitivity of future CMB experiment CMB-HD [80] which can measure the enhanced ΔN_{eff} due to light majoron. Next, we mark the threshold SNR $\varrho = 10$ for different detectors by the solid-colored curves, which shows the parameter ranges detectable by these GW detectors. From Fig. 6 and Fig. 5, it is clear that the BPs considered lie within the detectable ranges of almost all the GW detectors except ET. Note that even though the BP1 is allowed by the constraints that come from the indirect searches of the DM and also lies within the reach of different GW experiments, it still gets disallowed as it falls in the region of parameter space where the DW can overclose the Universe. Finally, the predictability of the model

is also enhanced as one of the BPs considered in Table II is already disfavored while other parameter space remain within reach of GW, CMB and DM indirect detection experiments. As can be seen from the summary plots shown in Fig. 6, the successful DM, DW and GW phenomenology requires the QG scale to be $\Lambda_{\text{QG}} \gtrsim 10^{21}$ GeV. The scale needs to be even higher for the GW emitted by DW annihilation to remain within experimental sensitivities. Such large QG scale can be natural in theories where the global symmetries are broken by non-perturbative instanton effects for example, D-brane in string theory [132–134] or gravitational instantons [135–138].

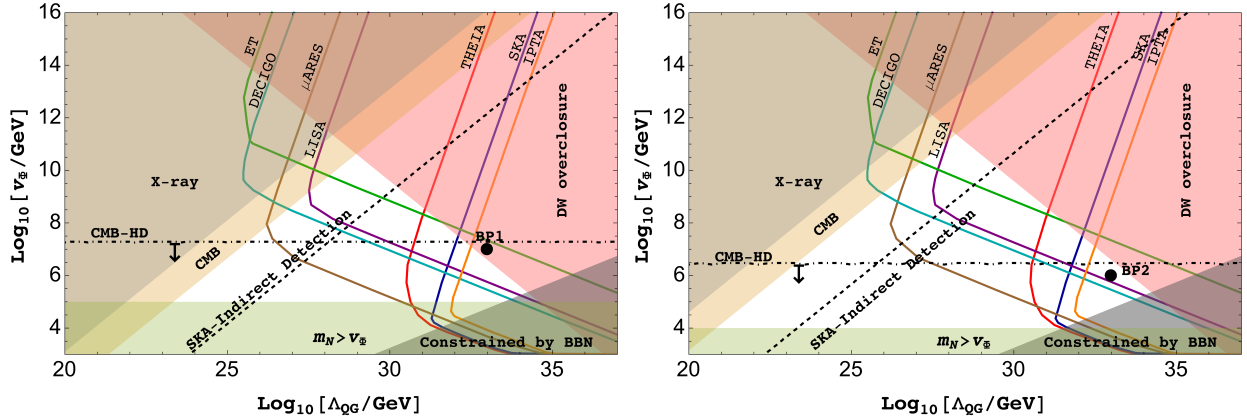


FIG. 6: Combined constraints on Λ_{QG} and v_Φ from indirect DM detection and GW observations with $\lambda_\Phi = 10^{-3}$. The light gray and yellow-shaded regions denote the excluded regions by X-ray and CMB observations respectively. The black dashed lines label the testing capabilities of the upcoming SKA telescope. The black dots correspond to the BPs shown in Table II. The red, blue, brown, cyan, purple, green, and orange curves correspond to the sensitivities of THEIA, SKA, μAres , DECIGO, LISA, ET, and IPTA with $\text{SNR} = 10$. The gray-shaded regions are excluded by the requirement of BBN. The pink-shaded region corresponds to the scenario where DW may overclose the Universe at an early epoch. The region below the horizontal dot-dashed line is within reach of CMB-HD experiment.

A. Analysis with dimension 7 operator

As seen from the above discussions, the lower bound on the QG scale from DM and DW requirements remains high because explicit Z_2 -breaking higher dimensional operators arise

at dimension five level in the minimal singlet majoron model. It is possible to have successful DM and GW phenomenology with a smaller QG scale if higher dimensional operators arise with dimensions more than five. While in the minimal model discussed in this work, we can not prevent dimension five operators suppressed by the QG scale, it is possible with additional gauge symmetries that prevent such operators up to certain dimensions. Similar ideas have already been adopted in the context of the axion quality problem [139–141]. Just for the demonstrative purpose, we consider a dimension 7 operator (as it also breaks the Z_2 symmetry explicitly) and write the energy bias after replacing field Φ with its VEV, this leads to a bias contribution to the effective potential of the form

$$V_{\text{bias}} \simeq \frac{v_\Phi^7}{\Lambda_{\text{QG}}^3}. \quad (29)$$

Following this, in Fig. 7, we set $\Lambda_{\text{QG}} = M_{\text{Pl}}$, where M_{Pl} denotes Planck mass and then we show the GW spectrum for different choices of the model parameters. Now from Eq. (24), we find that for the dimension 7 operator, $\Omega_p h^2 \propto (\lambda_\Phi^2 M_{\text{Pl}}^6)/v_\Phi^2$ and $f_p \propto v_\Phi^2/(\lambda_\Phi^{1/4} M_{\text{Pl}}^{3/2})$. Clearly, the presence of M_{Pl}^6 in numerator provides a huge enhancement in the peak amplitude for the dimension 7 operator. To compensate for such enhancement, a larger value of v_Φ together with a relatively smaller value of λ_Φ are required. Fig. 7 shows that with $v_\Phi \sim 10^{12}$ GeV, $\lambda_\Phi \sim 10^{-9}$ and $\Lambda_{\text{QG}} = M_{\text{Pl}}$, the GW spectrum generated by the DW annihilation remains within reach of different near future GW experiments.

Similar to Z_2 -breaking bias term, DM decay can also occur due to dimension 7 operator of the form

$$-\mathcal{L}_{\text{decay}} \supset \frac{Y_{D\alpha}}{\Lambda_{\text{QG}}^3} \overline{\ell_{L\alpha}} \tilde{H} \chi_R \Phi^3 + \text{h.c.}, \quad (30)$$

We choose a different benchmark point (BP3) to illustrate the combined result for DM and GW phenomenology. The chosen values for BP3 are : $v_\Phi = 10^{12}$ GeV, $\lambda_\Phi = 10^{-9}$, $m_N = 20$ GeV, $m_\chi = 20$ MeV, $\Lambda_{\text{QG}} = M_{\text{Pl}}$ and majoron mass in sub-eV scale. For BP3 the mass of ϕ is found to be $m_\phi = 4.5 \times 10^7$ GeV. Although to satisfy correct DM relic, it is sufficient to consider $2m_N < m_\phi$ as discussed in sub-section III A and III B, m_N around TeV scale requires a DM mass around GeV scale (e.g., $m_N = 10^4$ GeV requires $m_\chi \sim 1$ GeV). Now, a GeV scale DM mass along with $v_\Phi = 10^{12}$ GeV and $\Lambda_{\text{QG}} = M_{\text{Pl}}$ results in short DM lifetime in tension with indirect detection limits. Therefore, we choose a smaller $m_N = 20$ GeV and hence a smaller $m_\chi = 20$ MeV for BP3. The evolution of relevant number densities together with DM number density for BP3 are shown in the left plot of

Fig. 8. The final freeze-in abundance of DM, dominantly produced from decay, is consistent with the observed DM abundance. In the right panel of Fig. 8, we summarise our result for the dimension 7 operator. Here, we notice that the QG scale can be reduced to the Planck scale but only for a relatively large value of v_Φ and a smaller value of λ_Φ . Note that the price we pay to achieve the desired DM and GW phenomenology is a relatively small RHN mass (sub-TeV). As a result, its interaction with majoron becomes very feeble and the majorons never thermalises. This is the reason why we do not see the ΔN_{eff} bounds from thermalised majoron in Fig. 8. Despite this, the parameter space and BP3 in particular, remain within reach of near-future GW experiments like LISA and DM indirect detection experiments. While light majoron does not give rise to observable ΔN_{eff} in this scenario, higher dimensional operators can make majoron very heavy due to lower values of QG scale. If majoron becomes heavier than DM, we can have additional freeze-in contribution to DM relic. We find that this contribution is of same order as the contribution from the decay of ϕ without changing the generic conclusions. The details of majoron decay contribution to DM relic is given in appendix C.

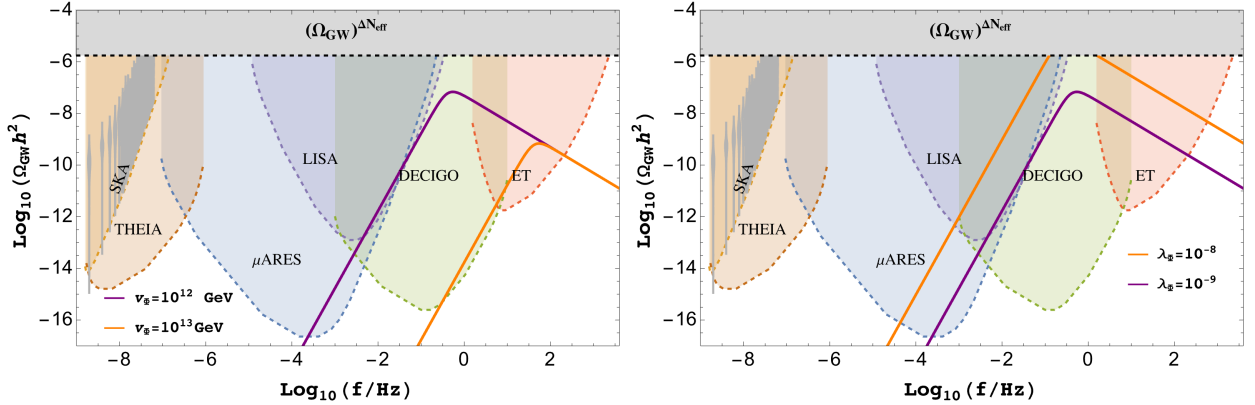


FIG. 7: The orange and purple curves show the GW spectrum generated from the annihilation of the DW. In both the panels we set $\Lambda_{\text{QG}} = M_{\text{Pl}}$ while fixing $\lambda_\Phi = 10^{-9}$ (left panel) and $v_\Phi = 10^{12}$ GeV (right panel). The gray color region denotes the portion excluded from ΔN_{eff} bound on energy density of GW.

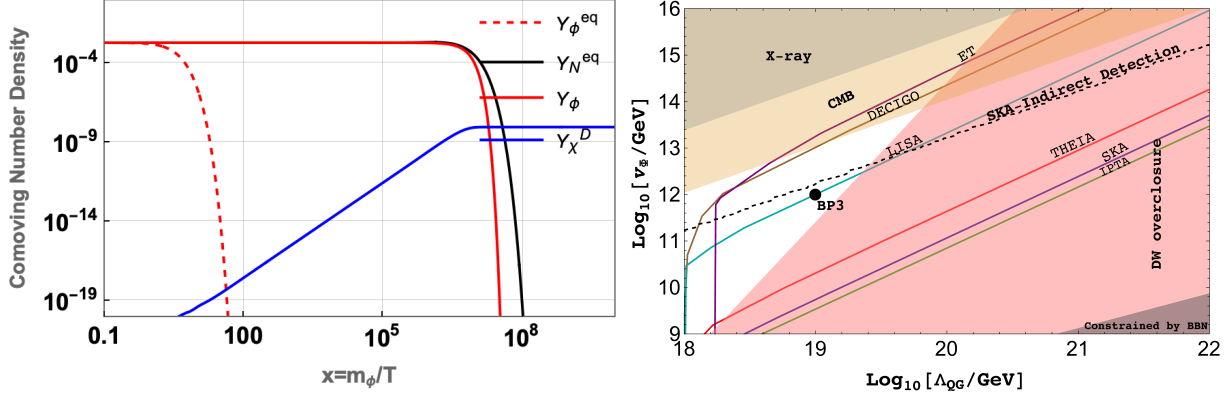


FIG. 8: Left panel: evolution of comoving number densities for BP3: $v_\phi = 10^{12}$ GeV, $\lambda_\phi = 10^{-9}$ (which gives $m_\phi = 4.5 \times 10^7$ GeV), $m_N = 20$ GeV and $m_\chi = 20$ MeV. Right panel: combined constraints on Λ_{QG} and v_ϕ with $\lambda_\phi = 10^{-9}$. The light gray and yellow-shaded regions denote the excluded regions by X-ray and CMB observations respectively with DM mass 20 MeV. The black dashed line shows the sensitivity of upcoming SKA telescope. The black dot corresponds to BP3. The red, blue, brown, cyan, purple, and green curves represent the sensitivities of THEIA, SKA, DECIGO, LISA, ET and IPTA with SNR = 10. The gray-shaded regions are excluded by the requirement of BBN. The pink-shaded region corresponds to the scenario where DW may overclose the Universe at an early epoch.

VI. CONCLUSION

We have studied the phenomenology of a dark matter scenario embedded in a global lepton number symmetry $U(1)_L$ focusing on the detection prospects. The spontaneous breaking of global lepton number symmetry generates right-handed neutrino mass or type-I seesaw scale dynamically. Explicit $U(1)_L$ breaking of the quadratic type not only leads to the mass of majoron, the pseudo-NG boson but also reduces the $U(1)_L$ symmetry to a Z_2 . The effective spontaneous breaking of Z_2 symmetry then leads to the formation of domain walls. We consider higher dimensional Z_2 -breaking operators suppressed by the QG scale as bias necessary for the domain walls to annihilate away while generating stochastic gravitational waves. The same QG scale-suppressed operators also lead to the decay of dark matter. In the minimal singlet majoron model, such QG scale suppressed operators can arise at dimension five level and get tightly constrained from DW, GW as well as DM lifetime criteria. These constraints make the non-thermal production of DM via singlet scalar portal couplings more

realistic. We consider the majoron to be in the sub-eV regime and produced thermally. This brings another detection prospect as light majoron can lead to observable ΔN_{eff} within reach of future CMB experiments. While the scale of QG is required to be $\Lambda_{\text{QG}} \gtrsim 10^{25}$ GeV for detectable GW from DW annihilation while satisfying indirect detection bounds on decaying DM, it can be brought down to the Planck scale if explicit global symmetry operators are considered at dimension 7 level instead of dimension 5.

To conclude, the minimal singlet majoron model provides a dynamical origin of the seesaw scale while also accommodating a stable DM without any additional discrete symmetries. The heavy right handed neutrinos not only generate light neutrino masses, but can also lead to successful leptogenesis with resonantly enhanced CP asymmetry. Quantum gravity effects, providing an origin of explicit global symmetry breaking, contribute to the generation of GW from domain wall annihilations while also opening up possible indirect detection aspects due to DM decay. Moreover, along with GW signatures, an observable ΔN_{eff} keeps the detection prospects of the model very promising while providing a common solution to the neutrino mass, dark matter and baryon asymmetry puzzles.

Acknowledgments

The work of D.B. is supported by the Science and Engineering Research Board (SERB), Government of India grants MTR/2022/000575 and CRG/2022/000603. D.B. also acknowledges the support from the Simons Foundation (Award Number:1023171-RC) to visit the International Institute of Physics, Natal, Brazil in May 2024 when part of this work was completed. R.R. acknowledges financial support from the STFC Consolidated Grant ST/T000775/1. The work of N.D. is supported by the Ministry of Education, Government of India via the Prime Minister's Research Fellowship (PMRF) December 2021 scheme. N.D. would like to thank Disha Bandyopadhyay for useful discussions. The authors would also like to express special thanks to the organisers of the Workshop in High Energy Physics Phenomenology (WHEPP XVII), IIT Gandhinagar, India where this project was initiated.

Appendix A: Coupling of CP-odd and CP-even scalars with N and χ

The interaction terms between Φ and N_R are

$$\frac{f_i}{2}\Phi\overline{N_{R_i}^c}N_{R_i} + \frac{f_i}{2}\Phi^*\overline{N_{R_i}}N_{R_i}^c. \quad (\text{A1})$$

Writing $N_i = N_{R_i} + N_{R_i}^c = P_R N_i + P_L N_i$, we get-

$$\frac{f_i}{2}\Phi\overline{P_L N_i}P_R N_i + \frac{f_i}{2}\Phi^*\overline{P_R N_i}P_L N_i = \frac{f_i}{2}\Phi\overline{N_i}P_R N_i + \frac{f_i}{2}\Phi^*\overline{N_i}P_L N_i.$$

After SSB, we can write $\Phi = \frac{1}{\sqrt{2}}(\phi + v_\Phi + i\eta)$. This gives -

$$\begin{aligned} & \frac{f_i}{2}\Phi\overline{N_i}P_R N_i + \frac{f_i}{2}\Phi^*\overline{N_i}P_L N_i \\ &= \frac{f_i}{2}\frac{1}{\sqrt{2}}(\phi + v_\Phi + i\eta)\overline{N_i}P_R N_i + \frac{f_i}{2}\frac{1}{\sqrt{2}}(\phi + v_\Phi - i\eta)\overline{N_i}P_L N_i \\ &= \frac{f_i}{2\sqrt{2}}\phi\overline{N_i}N_i + \frac{f_i}{2\sqrt{2}}v_\Phi\overline{N_i}N_i + i\frac{f_i}{2\sqrt{2}}\eta\overline{N_i}\gamma^5 N_i. \end{aligned} \quad (\text{A2})$$

Similarly the interaction terms between Φ and DM give -

$$\begin{aligned} & y_\chi\Phi\overline{\chi_L}\chi_R + y_\chi\Phi^*\overline{\chi_R}\chi_L \\ &= \frac{y_\chi}{\sqrt{2}}\phi\overline{\chi}\chi + \frac{y_\chi}{\sqrt{2}}v_\Phi\overline{\chi}\chi + i\frac{y_\chi}{\sqrt{2}}\eta\overline{\chi}\gamma^5\chi, \end{aligned} \quad (\text{A3})$$

where $\chi = \chi_L + \chi_R$.

Appendix B: Cross-section

Here we provide the expressions for relevant cross-sections used in the numerical analysis.

$$\begin{aligned} (\sigma v)_{N\eta \rightarrow N\eta} &= \frac{f^4}{2048\pi \left((m_\eta^2 + m_N^2 - s)^2 - 4m_\eta^2 m_N^2 \right)} \left(\frac{(-2m_N^2(m_\eta^2 + s) + m_N^4 + (s - m_\eta^2))}{s^2} \times \right. \\ & \left(-2m_\eta^2 + \frac{m_\eta^4(s - m_N^2)^2(sm_N^2 + m_N^4 + 2s^2) + 2m_\eta^{10}(m_N^2 + s) - m_\eta^8(m_N^2 + s)(3m_N^2 + s)}{(s - m_N^2)^2 \left(2m_\eta^6 - m_\eta^4(3m_N^2 + s) + (m_N^3 - sm_N)^2 \right)} \right. \\ & \left. \left. + m_N^2 + 5s \right) - \frac{2(2m_\eta^4 + (s - m_N^2)^2)}{s - m_N^2} \log \left(\frac{m_\eta^4 - m_N^2(2m_\eta^2 + s) + m_N^4}{s(2m_\eta^2 + m_N^2 - s)} \right) \right). \end{aligned} \quad (\text{B1})$$

$$\begin{aligned}
(\sigma v)_{\phi\phi\rightarrow N\bar{N}} = & -\frac{f^4}{512\pi s (s - 4m_\phi^2)} \times \\
& \left(s \sqrt{\frac{(s - 4m_N^2)(s - 4m_\phi^2)}{s^2}} + (8m_N^2 - 2m_\phi^2 + s) \log \left(\frac{s \left(\sqrt{\frac{(s - 4m_N^2)(s - 4m_\phi^2)}{s^2}} - 1 \right) + 2m_\phi^2}{2m_\phi^2 - s \left(\sqrt{\frac{(s - 4m_N^2)(s - 4m_\phi^2)}{s^2}} + 1 \right)} \right) \right. \\
& + \frac{s (16m_N^4 + m_N^2 (s - 12m_\phi^2) + 2m_\phi^4) \sqrt{\frac{(s - 4m_N^2)(s - 4m_\phi^2)}{s^2}}}{m_N^2 (s - 4m_\phi^2) + m_\phi^4} \\
& \left. - \frac{2 (-16m_N^4 + 4m_N^2 s + m_\phi^4) \log \left(\frac{s \left(\sqrt{\frac{(s - 4m_N^2)(s - 4m_\phi^2)}{s^2}} - 1 \right) + 2m_\phi^2}{2m_\phi^2 - s \left(\sqrt{\frac{(s - 4m_N^2)(s - 4m_\phi^2)}{s^2}} + 1 \right)} \right)}{2m_\phi^2 - s} \right). \tag{B2}
\end{aligned}$$

Appendix C: Dark matter from Majoron decay

In this work, we have focused on light majorons which remain relativistic during recombination and contribute to ΔN_{eff} . Therefore, we have kept the soft $U(1)_L$ breaking mass term in the sub-eV range. However, higher dimensional operators suppressed by powers of Λ_{QG} can push the majoron to higher masses. In the minimal model with dimension five operators suppressed by Λ_{QG} , the next-to-leading-order (NLO) contribution to majoron mass is $\sim \sqrt{v_\Phi^3/\Lambda_{\text{QG}}}$. For some parts of the parameter space, this contribution can be kept at or below eV scale while for the rest of the parameter space, some tuning will be required between bare mass and NLO mass such that the net majoron mass remains at or below the eV scale. This keeps the ΔN_{eff} prospects alive as discussed above.

On the other hand, for lower values of Λ_{QG} as applicable in a scenario where NLO terms arise at dimension seven order, majoron mass $\sim \sqrt{v_\Phi^5/\Lambda_{\text{QG}}^3}$ can become substantially large. Since we do not have observable ΔN_{eff} in the scenario with dimension seven operators as discussed earlier, we do not lose any interesting phenomenology if majorons become heavy and non-relativistic due to NLO operators. However, if majorons become even heavier than DM that is, $m_\eta > 2m_\chi$, majoron can decay to DM and contribute to the DM abundance. The coupled BEs for majoron and DM can be written as

$$\frac{dY_\eta}{dx} = -\frac{\beta s}{\mathcal{H}x} \langle \sigma v \rangle_{\eta\eta \rightarrow N\bar{N}} (Y_\eta^2 - (Y_\eta^{\text{eq}})^2) - \frac{\beta}{\mathcal{H}x} \Gamma_{\eta \rightarrow N\bar{N}} \frac{K_1(m_\eta/T)}{K_2(m_\eta/T)} (Y_\eta - Y_\eta^{\text{eq}}) \quad (\text{C1})$$

$$-\frac{\beta}{\mathcal{H}x} \Gamma_{\eta \rightarrow \chi\bar{\chi}} \frac{K_1(m_\eta/T)}{K_2(m_\eta/T)} Y_\eta,$$

$$\frac{dY_\chi}{dx} = \frac{\beta}{\mathcal{H}x} \Gamma_{\phi \rightarrow \chi\bar{\chi}} \frac{K_1(m_\phi/T)}{K_2(m_\phi/T)} Y_\phi + \frac{\beta}{\mathcal{H}x} \Gamma_{\eta \rightarrow \chi\bar{\chi}} \frac{K_1(m_\eta/T)}{K_2(m_\eta/T)} Y_\eta + \frac{\beta s}{\mathcal{H}x} \langle \sigma v \rangle_{N\bar{N} \rightarrow \chi\bar{\chi}} (Y_N^{\text{eq}})^2. \quad (\text{C2})$$

To compare the production of DM from majoron decay and from ϕ decay, we plot the comoving number densities for BP3 in Fig. 9. For BP3, $v_\Phi = 10^{12}$ GeV, $\lambda_\Phi = 10^{-9}$ ($m_\phi = 4.5 \times 10^7$ GeV), $m_N = 20$ GeV, $m_\chi = 20$ MeV, $\Lambda_{\text{QG}} = M_{\text{Pl}}$. The majoron mass is determined by the dimension 7 operator which is calculated as $m_\eta = \sqrt{\frac{21}{4\sqrt{2}} \frac{v_\Phi^5}{\Lambda_{\text{QG}}^3}} \simeq 61$ GeV. Fig. 9 shows that the DM yield from ϕ and majoron η decay by solid blue and dashed blue lines respectively. About equal amount of DM is produced from both the ϕ and majoron decay as the branching ratio of $\phi \rightarrow \chi\bar{\chi}$ and $\eta \rightarrow \chi\bar{\chi}$ are similar. However, the production of DM from majoron decay is delayed compared to ϕ decay due to smaller decay width of majoron.

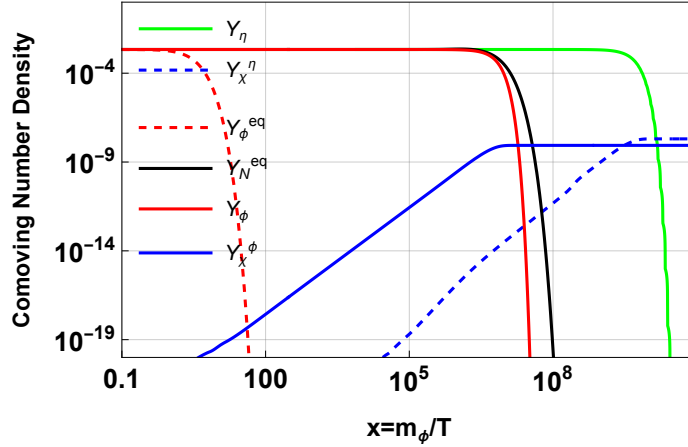


FIG. 9: Evolution of comoving number densities of different species for BP3. The solid red and solid green color lines denote the evolution of ϕ and η respectively. DM abundance from ϕ and majoron decay are denoted by solid blue and dashed blue color lines respectively. Both ϕ and majoron decay contribute at the same order to the DM abundances as depicted in the figure.

- 2020** (2020), no. 8 083C01.
- [2] **Planck** Collaboration, N. Aghanim et al., *Planck 2018 results. VI. Cosmological parameters*, *Astron. Astrophys.* **641** (2020) A6, [[arXiv:1807.06209](#)]. [Erratum: *Astron. Astrophys.* 652, C4 (2021)].
 - [3] P. Minkowski, $\mu \rightarrow e\gamma$ at a Rate of One Out of 10^9 Muon Decays?, *Phys. Lett. B* **67** (1977) 421–428.
 - [4] M. Gell-Mann, P. Ramond, and R. Slansky, *Complex Spinors and Unified Theories*, *Conf. Proc. C* **790927** (1979) 315–321, [[arXiv:1306.4669](#)].
 - [5] R. N. Mohapatra and G. Senjanovic, *Neutrino Mass and Spontaneous Parity Nonconservation*, *Phys. Rev. Lett.* **44** (1980) 912.
 - [6] O. Sawada and A. Sugamoto, eds., *Proceedings: Workshop on the Unified Theories and the Baryon Number in the Universe: Tsukuba, Japan, February 13-14, 1979*, (Tsukuba, Japan), Natl.Lab.High Energy Phys., 1979.
 - [7] T. Yanagida, *Horizontal Symmetry and Masses of Neutrinos*, *Prog. Theor. Phys.* **64** (1980) 1103.
 - [8] J. Schechter and J. Valle, *Neutrino Masses in $SU(2) \times U(1)$ Theories*, *Phys. Rev. D* **22** (1980) 2227.
 - [9] G. Arcadi, M. Dutra, P. Ghosh, M. Lindner, Y. Mambrini, M. Pierre, S. Profumo, and F. S. Queiroz, *The waning of the WIMP? A review of models, searches, and constraints*, *Eur. Phys. J. C* **78** (2018), no. 3 203, [[arXiv:1703.07364](#)].
 - [10] N. Bernal, M. Heikinheimo, T. Tenkanen, K. Tuominen, and V. Vaskonen, *The Dawn of FIMP Dark Matter: A Review of Models and Constraints*, *Int. J. Mod. Phys. A* **32** (2017), no. 27 1730023, [[arXiv:1706.07442](#)].
 - [11] S. Weinberg, *Cosmological Production of Baryons*, *Phys. Rev. Lett.* **42** (1979) 850–853.
 - [12] E. W. Kolb and S. Wolfram, *Baryon Number Generation in the Early Universe*, *Nucl. Phys.* **B172** (1980) 224. [Erratum: *Nucl. Phys.* B195,542(1982)].
 - [13] M. Fukugita and T. Yanagida, *Baryogenesis Without Grand Unification*, *Phys. Lett. B* **174** (1986) 45–47.
 - [14] V. A. Kuzmin, V. A. Rubakov, and M. E. Shaposhnikov, *On the Anomalous Electroweak Baryon Number Nonconservation in the Early Universe*, *Phys. Lett.* **155B** (1985) 36.
 - [15] **LUX-ZEPLIN** Collaboration, J. Aalbers et al., *First Dark Matter Search Results from the*

- LUX-ZEPLIN (LZ) Experiment*, [arXiv:2207.03764](#).
- [16] J. A. Dror, T. Hiramatsu, K. Kohri, H. Murayama, and G. White, *Testing the Seesaw Mechanism and Leptogenesis with Gravitational Waves*, *Phys. Rev. Lett.* **124** (2020), no. 4 041804, [[arXiv:1908.03227](#)].
 - [17] S. Blasi, V. Brdar, and K. Schmitz, *Fingerprint of low-scale leptogenesis in the primordial gravitational-wave spectrum*, *Phys. Rev. Res.* **2** (2020), no. 4 043321, [[arXiv:2004.02889](#)].
 - [18] B. Fornal and B. Shams Es Haghi, *Baryon and Lepton Number Violation from Gravitational Waves*, *Phys. Rev. D* **102** (2020), no. 11 115037, [[arXiv:2008.05111](#)].
 - [19] R. Samanta and S. Datta, *Gravitational wave complementarity and impact of NANOGrav data on gravitational leptogenesis*, *JHEP* **05** (2021) 211, [[arXiv:2009.13452](#)].
 - [20] B. Barman, D. Borah, A. Dasgupta, and A. Ghoshal, *Probing High Scale Dirac Leptogenesis via Gravitational Waves from Domain Walls*, [arXiv:2205.03422](#).
 - [21] P. Huang and K.-P. Xie, *Leptogenesis triggered by a first-order phase transition*, [arXiv:2206.04691](#).
 - [22] A. Dasgupta, P. S. B. Dev, A. Ghoshal, and A. Mazumdar, *Gravitational Wave Pathway to Testable Leptogenesis*, [arXiv:2206.07032](#).
 - [23] N. Okada and O. Seto, *Probing the seesaw scale with gravitational waves*, *Phys. Rev. D* **98** (2018), no. 6 063532, [[arXiv:1807.00336](#)].
 - [24] T. Hasegawa, N. Okada, and O. Seto, *Gravitational waves from the minimal gauged $U(1)_{B-L}$ model*, *Phys. Rev. D* **99** (2019), no. 9 095039, [[arXiv:1904.03020](#)].
 - [25] D. Borah, A. Dasgupta, and I. Saha, *Leptogenesis and dark matter through relativistic bubble walls with observable gravitational waves*, *JHEP* **11** (2022) 136, [[arXiv:2207.14226](#)].
 - [26] D. Borah, S. Jyoti Das, and R. Roshan, *Probing high scale seesaw and PBH generated dark matter via gravitational waves with multiple tilts*, *Nucl. Phys. B* **1002** (2024) 116528, [[arXiv:2208.04965](#)].
 - [27] B. Barman, D. Borah, S. Jyoti Das, and I. Saha, *Scale of Dirac leptogenesis and left-right symmetry in the light of recent PTA results*, *JCAP* **10** (2023) 053, [[arXiv:2307.00656](#)].
 - [28] D. Borah, A. Dasgupta, and I. Saha, *LIGO-VIRGO constraints on dark matter and leptogenesis triggered by a first order phase transition at high scale*, [arXiv:2304.08888](#).
 - [29] K. Saikawa, *A review of gravitational waves from cosmic domain walls*, *Universe* **3** (2017), no. 2 40, [[arXiv:1703.02576](#)].

- [30] R. Roshan and G. White, *Using gravitational waves to see the first second of the Universe*, [arXiv:2401.04388](#).
- [31] S. Bhattacharya, N. Mondal, R. Roshan, and D. Vatsyayan, *Testing the dark and visible sides of the Seesaw*, [arXiv:2312.15053](#).
- [32] S. Blasi, A. Mariotti, A. Rase, A. Sevrin, and K. Turbang, *Friction on ALP domain walls and gravitational waves*, *JCAP* **04** (2023) 008, [[arXiv:2210.14246](#)].
- [33] S. Blasi, A. Mariotti, A. Rase, and A. Sevrin, *Axionic domain walls at Pulsar Timing Arrays: QCD bias and particle friction*, *JHEP* **11** (2023) 169, [[arXiv:2306.17830](#)].
- [34] S. F. King, R. Roshan, X. Wang, G. White, and M. Yamazaki, *Quantum gravity effects on dark matter and gravitational waves*, *Phys. Rev. D* **109** (2024), no. 2 024057, [[arXiv:2308.03724](#)].
- [35] S. F. King, R. Roshan, X. Wang, G. White, and M. Yamazaki, *Quantum Gravity Effects on Fermionic Dark Matter and Gravitational Waves*, [arXiv:2311.12487](#).
- [36] D. Borah and A. Dasgupta, *Probing left-right symmetry via gravitational waves from domain walls*, *Phys. Rev. D* **106** (2022), no. 3 035016, [[arXiv:2205.12220](#)].
- [37] Y. Chikashige, R. N. Mohapatra, and R. D. Peccei, *Spontaneously Broken Lepton Number and Cosmological Constraints on the Neutrino Mass Spectrum*, *Phys. Rev. Lett.* **45** (1980) 1926.
- [38] Y. Chikashige, R. N. Mohapatra, and R. D. Peccei, *Are There Real Goldstone Bosons Associated with Broken Lepton Number?*, *Phys. Lett. B* **98** (1981) 265–268.
- [39] G. B. Gelmini and M. Roncadelli, *Left-Handed Neutrino Mass Scale and Spontaneously Broken Lepton Number*, *Phys. Lett. B* **99** (1981) 411–415.
- [40] S. K. Manna and A. Sil, *Majorons revisited: Light dark matter as a FIMP*, *Phys. Rev. D* **108** (2023), no. 7 075026, [[arXiv:2212.08404](#)].
- [41] G. 't Hooft, *Symmetry Breaking Through Bell-Jackiw Anomalies*, *Phys. Rev. Lett.* **37** (1976) 8–11.
- [42] G. Lazarides, M. Reig, Q. Shafi, R. Srivastava, and J. W. F. Valle, *Spontaneous Breaking of Lepton Number and the Cosmological Domain Wall Problem*, *Phys. Rev. Lett.* **122** (2019), no. 15 151301, [[arXiv:1806.11198](#)].
- [43] T. Brune, *Leptogenesis in Majoron models without domain walls*, *Phys. Rev. D* **107** (2023), no. 9 096023, [[arXiv:2201.12239](#)].

- [44] Y. B. Zeldovich, I. Y. Kobzarev, and L. B. Okun, *Cosmological Consequences of the Spontaneous Breakdown of Discrete Symmetry*, *Zh. Eksp. Teor. Fiz.* **67** (1974) 3–11.
- [45] T. W. B. Kibble, *Topology of Cosmic Domains and Strings*, *J. Phys. A* **9** (1976) 1387–1398.
- [46] A. Vilenkin, *Gravitational Field of Vacuum Domain Walls and Strings*, *Phys. Rev. D* **23** (1981) 852–857.
- [47] B. Fu, A. Ghoshal, and S. F. King, *Cosmic string gravitational waves from global $U(1)_{B-L}$ symmetry breaking as a probe of the type I seesaw scale*, *JHEP* **11** (2023) 071, [[arXiv:2306.07334](#)].
- [48] J. Baeza-Ballesteros, E. J. Copeland, D. G. Figueroa, and J. Lizarraga, *Gravitational Wave Emission from a Cosmic String Loop, I: Global Case*, [arXiv:2308.08456](#).
- [49] Y. Wu, K.-P. Xie, and Y.-L. Zhou, *Collapsing domain walls beyond Z_2* , *Phys. Rev. D* **105** (2022), no. 9 095013, [[arXiv:2204.04374](#)].
- [50] Y. Wu, K.-P. Xie, and Y.-L. Zhou, *Classification of Abelian domain walls*, *Phys. Rev. D* **106** (2022), no. 7 075019, [[arXiv:2205.11529](#)].
- [51] Y. Bai, T.-K. Chen, and M. Korwar, *QCD-collapsed domain walls: QCD phase transition and gravitational wave spectroscopy*, *JHEP* **12** (2023) 194, [[arXiv:2306.17160](#)].
- [52] P.-H. Gu, E. Ma, and U. Sarkar, *Pseudo-Majoron as Dark Matter*, *Phys. Lett. B* **690** (2010) 145–148, [[arXiv:1004.1919](#)].
- [53] F. S. Queiroz and K. Sinha, *The Poker Face of the Majoron Dark Matter Model: LUX to keV Line*, *Phys. Lett. B* **735** (2014) 69–74, [[arXiv:1404.1400](#)].
- [54] R. Kallosh, A. D. Linde, D. A. Linde, and L. Susskind, *Gravity and global symmetries*, *Phys. Rev. D* **52** (1995) 912–935, [[hep-th/9502069](#)].
- [55] E. Witten, *Symmetry and Emergence*, *Nature Phys.* **14** (2018), no. 2 116–119, [[arXiv:1710.01791](#)].
- [56] B. Rai and G. Senjanovic, *Gravity and domain wall problem*, *Phys. Rev. D* **49** (1994) 2729–2733, [[hep-ph/9301240](#)].
- [57] K. A. Beyer and S. Sarkar, *Ruling out light axions: The writing is on the wall*, *SciPost Phys.* **15** (2023), no. 1 003, [[arXiv:2211.14635](#)].
- [58] J. Preskill, M. B. Wise, and F. Wilczek, *Cosmology of the Invisible Axion*, *Phys. Lett. B* **120** (1983) 127–132.
- [59] L. F. Abbott and P. Sikivie, *A Cosmological Bound on the Invisible Axion*, *Phys. Lett. B*

- 120** (1983) 133–136.
- [60] M. Dine and W. Fischler, *The Not So Harmless Axion*, *Phys. Lett. B* **120** (1983) 137–141.
 - [61] R. T. Co, L. J. Hall, and K. Harigaya, *Axion Kinetic Misalignment Mechanism*, *Phys. Rev. Lett.* **124** (2020), no. 25 251802, [[arXiv:1910.14152](#)].
 - [62] I. Affleck and M. Dine, *A New Mechanism for Baryogenesis*, *Nucl. Phys. B* **249** (1985) 361–380.
 - [63] A. G. Cohen and D. B. Kaplan, *Thermodynamic Generation of the Baryon Asymmetry*, *Phys. Lett. B* **199** (1987) 251–258.
 - [64] A. G. Cohen and D. B. Kaplan, *SPONTANEOUS BARYOGENESIS*, *Nucl. Phys. B* **308** (1988) 913–928.
 - [65] R. T. Co and K. Harigaya, *Axiogenesis*, *Phys. Rev. Lett.* **124** (2020), no. 11 111602, [[arXiv:1910.02080](#)].
 - [66] E. J. Chun and T. H. Jung, *Leptogenesis driven by a Majoron*, *Phys. Rev. D* **109** (2024), no. 9 095004, [[arXiv:2311.09005](#)].
 - [67] M. Ibe and K. Kaneta, *Spontaneous thermal Leptogenesis via Majoron oscillation*, *Phys. Rev. D* **92** (2015), no. 3 035019, [[arXiv:1504.04125](#)].
 - [68] V. Domcke, Y. Ema, K. Mukaida, and M. Yamada, *Spontaneous Baryogenesis from Axions with Generic Couplings*, *JHEP* **08** (2020) 096, [[arXiv:2006.03148](#)].
 - [69] R. T. Co, T. Gherghetta, and K. Harigaya, *Axiogenesis with a heavy QCD axion*, *JHEP* **10** (2022) 121, [[arXiv:2206.00678](#)].
 - [70] M. Berbig, *Diraxiogenesis*, *JHEP* **01** (2024) 061, [[arXiv:2307.14121](#)].
 - [71] R. T. Co, N. Fernandez, A. Ghalsasi, L. J. Hall, and K. Harigaya, *Lepto-Axiogenesis*, *JHEP* **03** (2021) 017, [[arXiv:2006.05687](#)].
 - [72] W. Chao and Y.-Q. Peng, *Majorana Majoron and the Baryon Asymmetry of the Universe*, [arXiv:2311.06469](#).
 - [73] P. Barnes, R. T. Co, K. Harigaya, and A. Pierce, *Lepto-axiogenesis with light right-handed neutrinos*, [arXiv:2402.10263](#).
 - [74] G. Barenboim, P. Ko, and W.-i. Park, *The minimal cosmological standard model*, [arXiv:2403.05390](#).
 - [75] G. Barenboim, P. Ko, and W.-i. Park, *Axi-majoron for almost everything*, [arXiv:2403.08675](#).

- [76] A. Datta, S. K. Manna, and A. Sil, *Spontaneous Leptogenesis with sub-GeV Axion Like Particles*, [arXiv:2405.07003](#).
- [77] R. T. Co, N. Fernandez, A. Ghalsasi, K. Harigaya, and J. Shelton, *Axion baryogenesis puts a new spin on the Hubble tension*, [arXiv:2405.12268](#).
- [78] K. Akita and M. Niibo, *Updated constraints and future prospects on majoron dark matter*, *JHEP* **07** (2023) 132, [[arXiv:2304.04430](#)].
- [79] A. de Giorgi, L. Merlo, X. Ponce Díaz, and S. Rigolin, *The minimal massive Majoron Seesaw Model*, *JHEP* **03** (2024) 094, [[arXiv:2312.13417](#)].
- [80] **CMB-HD** Collaboration, S. Aiola et al., *Snowmass2021 CMB-HD White Paper*, [arXiv:2203.05728](#).
- [81] M. Reig, J. W. F. Valle, and M. Yamada, *Light majoron cold dark matter from topological defects and the formation of boson stars*, *JCAP* **09** (2019) 029, [[arXiv:1905.01287](#)].
- [82] K. Griest and M. Kamionkowski, *Unitarity Limits on the Mass and Radius of Dark Matter Particles*, *Phys. Rev. Lett.* **64** (1990) 615.
- [83] L. J. Hall, K. Jedamzik, J. March-Russell, and S. M. West, *Freeze-In Production of FIMP Dark Matter*, *JHEP* **03** (2010) 080, [[arXiv:0911.1120](#)].
- [84] Q. Decant, J. Heisig, D. C. Hooper, and L. Lopez-Honorez, *Lyman- α constraints on freeze-in and superWIMPs*, *JCAP* **03** (2022) 041, [[arXiv:2111.09321](#)].
- [85] A. Biswas, D. Borah, N. Das, and D. Nanda, *Freeze-in dark matter via a light Dirac neutrino portal*, *Phys. Rev. D* **107** (2023), no. 1 015015, [[arXiv:2205.01144](#)].
- [86] S. Tremaine and J. E. Gunn, *Dynamical role of light neutral leptons in cosmology*, *Phys. Rev. Lett.* **42** (Feb, 1979) 407–410.
- [87] S. Blanchet and P. Di Bari, *Flavor effects on leptogenesis predictions*, *JCAP* **03** (2007) 018, [[hep-ph/0607330](#)].
- [88] P. S. B. Dev, P. Di Bari, B. Garbrecht, S. Lavignac, P. Millington, and D. Teresi, *Flavor effects in leptogenesis*, *Int. J. Mod. Phys. A* **33** (2018) 1842001, [[arXiv:1711.02861](#)].
- [89] A. Pilaftsis and T. E. J. Underwood, *Resonant leptogenesis*, *Nucl. Phys. B* **692** (2004) 303–345, [[hep-ph/0309342](#)].
- [90] A. Datta, R. Roshan, and A. Sil, *Imprint of the Seesaw Mechanism on Feebly Interacting Dark Matter and the Baryon Asymmetry*, *Phys. Rev. Lett.* **127** (2021), no. 23 231801, [[arXiv:2104.02030](#)].

- [91] R. E. Shrock, *Electromagnetic Properties and Decays of Dirac and Majorana Neutrinos in a General Class of Gauge Theories*, *Nucl. Phys. B* **206** (1982) 359–379.
- [92] R. Essig, E. Kuflik, S. D. McDermott, T. Volansky, and K. M. Zurek, *Constraining Light Dark Matter with Diffuse X-Ray and Gamma-Ray Observations*, *JHEP* **11** (2013) 193, [[arXiv:1309.4091](#)].
- [93] O. Ruchayskiy and A. Ivashko, *Experimental bounds on sterile neutrino mixing angles*, *JHEP* **06** (2012) 100, [[arXiv:1112.3319](#)].
- [94] D. E. Gruber, J. L. Matteson, L. E. Peterson, and G. V. Jung, *The spectrum of diffuse cosmic hard x-rays measured with heao-1*, *Astrophys. J.* **520** (1999) 124, [[astro-ph/9903492](#)].
- [95] L. Bouchet, E. Jourdain, J. P. Roques, A. Strong, R. Diehl, F. Lebrun, and R. Terrier, *INTEGRAL SPI All-Sky View in Soft Gamma Rays: Study of Point Source and Galactic Diffuse Emissions*, *Astrophys. J.* **679** (2008) 1315, [[arXiv:0801.2086](#)].
- [96] P. Sreekumar, F. W. Stecker, and S. C. Kappadath, *The extragalactic diffuse gamma-ray emission*, *AIP Conf. Proc.* **410** (1997), no. 1 344, [[astro-ph/9709258](#)].
- [97] A. W. Strong, I. V. Moskalenko, and O. Reimer, *Evaluation of models for diffuse continuum gamma-rays in EGRET range*, in *28th International Cosmic Ray Conference*, pp. 2309–2312, 6, 2003. [astro-ph/0306346](#).
- [98] A. Boyarsky, O. Ruchayskiy, and M. Shaposhnikov, *The Role of sterile neutrinos in cosmology and astrophysics*, *Ann. Rev. Nucl. Part. Sci.* **59** (2009) 191–214, [[arXiv:0901.0011](#)].
- [99] **Fermi-LAT** Collaboration, M. Ackermann et al., *Constraints on the Galactic Halo Dark Matter from Fermi-LAT Diffuse Measurements*, *Astrophys. J.* **761** (2012) 91, [[arXiv:1205.6474](#)].
- [100] **Fermi-LAT** Collaboration, M. Ackermann et al., *Fermi LAT Search for Dark Matter in Gamma-ray Lines and the Inclusive Photon Spectrum*, *Phys. Rev. D* **86** (2012) 022002, [[arXiv:1205.2739](#)].
- [101] **Fermi-LAT** Collaboration, M. Ackermann et al., *Updated search for spectral lines from Galactic dark matter interactions with pass 8 data from the Fermi Large Area Telescope*, *Phys. Rev. D* **91** (2015), no. 12 122002, [[arXiv:1506.00013](#)].
- [102] J. F. Navarro, C. S. Frenk, and S. D. M. White, *The Structure of cold dark matter halos*,

- Astrophys. J.* **462** (1996) 563–575, [[astro-ph/9508025](#)].
- [103] **WMAP** Collaboration, G. Hinshaw et al., *Nine-Year Wilkinson Microwave Anisotropy Probe (WMAP) Observations: Cosmological Parameter Results*, *Astrophys. J. Suppl.* **208** (2013) 19, [[arXiv:1212.5226](#)].
 - [104] **ACTPol** Collaboration, S. Naess et al., *The Atacama Cosmology Telescope: CMB Polarization at $200 < \ell < 9000$* , *JCAP* **10** (2014) 007, [[arXiv:1405.5524](#)].
 - [105] Z. Hou et al., *Constraints on Cosmology from the Cosmic Microwave Background Power Spectrum of the 2500 deg² SPT-SZ Survey*, *Astrophys. J.* **782** (2014) 74, [[arXiv:1212.6267](#)].
 - [106] T. R. Slatyer and C.-L. Wu, *General Constraints on Dark Matter Decay from the Cosmic Microwave Background*, *Phys. Rev. D* **95** (2017), no. 2 023010, [[arXiv:1610.06933](#)].
 - [107] S. Colafrancesco, M. Regis, P. Marchegiani, G. Beck, R. Beck, H. Zechlin, A. Lobanov, and D. Horns, *Probing the nature of Dark Matter with the SKA*, *PoS AASKA14* (2015) 100, [[arXiv:1502.03738](#)].
 - [108] K. Dutta, A. Ghosh, A. Kar, and B. Mukhopadhyaya, *A general study of decaying scalar dark matter: existing limits and projected radio signals at the SKA*, *JCAP* **09** (2022) 005, [[arXiv:2204.06024](#)].
 - [109] W. H. Press, B. S. Ryden, and D. N. Spergel, *Dynamical Evolution of Domain Walls in an Expanding Universe*, *Astrophys. J.* **347** (1989) 590–604.
 - [110] T. Garagounis and M. Hindmarsh, *Scaling in numerical simulations of domain walls*, *Phys. Rev. D* **68** (2003) 103506, [[hep-ph/0212359](#)].
 - [111] J. C. R. E. Oliveira, C. J. A. P. Martins, and P. P. Avelino, *The Cosmological evolution of domain wall networks*, *Phys. Rev. D* **71** (2005) 083509, [[hep-ph/0410356](#)].
 - [112] A. Leite and C. Martins, *Scaling Properties of Domain Wall Networks*, *Phys. Rev. D* **84** (2011) 103523, [[arXiv:1110.3486](#)].
 - [113] A. M. M. Leite, C. J. A. P. Martins, and E. P. S. Shellard, *Accurate Calibration of the Velocity-dependent One-scale Model for Domain Walls*, *Phys. Lett. B* **718** (2013) 740–744, [[arXiv:1206.6043](#)].
 - [114] T. Hiramatsu, M. Kawasaki, and K. Saikawa, *On the estimation of gravitational wave spectrum from cosmic domain walls*, *JCAP* **02** (2014) 031, [[arXiv:1309.5001](#)].
 - [115] G. B. Gelmini, M. Gleiser, and E. W. Kolb, *Cosmology of Biased Discrete Symmetry Breaking*, *Phys. Rev. D* **39** (1989) 1558.

- [116] S. E. Larsson, S. Sarkar, and P. L. White, *Evading the cosmological domain wall problem*, *Phys. Rev. D* **55** (1997) 5129–5135, [[hep-ph/9608319](#)].
- [117] T. Hiramatsu, M. Kawasaki, K. Saikawa, and T. Sekiguchi, *Axion cosmology with long-lived domain walls*, *JCAP* **01** (2013) 001, [[arXiv:1207.3166](#)].
- [118] N. Chen, T. Li, and Y. Wu, *The gravitational waves from the collapsing domain walls in the complex singlet model*, *JHEP* **08** (2020) 117, [[arXiv:2004.10148](#)].
- [119] C. Caprini et al., *Detecting gravitational waves from cosmological phase transitions with LISA: an update*, *JCAP* **03** (2020) 024, [[arXiv:1910.13125](#)].
- [120] **NANOGrav** Collaboration, A. Afzal et al., *The NANOGrav 15 yr Data Set: Search for Signals from New Physics*, *Astrophys. J. Lett.* **951** (2023), no. 1 L11, [[arXiv:2306.16219](#)].
- [121] G. Domènech, C. Lin, and M. Sasaki, *Gravitational wave constraints on the primordial black hole dominated early universe*, *JCAP* **04** (2021) 062, [[arXiv:2012.08151](#)]. [Erratum: *JCAP* **11**, E01 (2021)].
- [122] M. Punturo et al., *The Einstein Telescope: A third-generation gravitational wave observatory*, *Class. Quant. Grav.* **27** (2010) 194002.
- [123] **LISA** Collaboration, P. Amaro-Seoane et al., *Laser Interferometer Space Antenna*, [arXiv:1702.00786](#).
- [124] S. Kawamura et al., *Current status of space gravitational wave antenna DECIGO and B-DECIGO*, *PTEP* **2021** (2021), no. 5 05A105, [[arXiv:2006.13545](#)].
- [125] A. Sesana et al., *Unveiling the gravitational universe at μ -Hz frequencies*, *Exper. Astron.* **51** (2021), no. 3 1333–1383, [[arXiv:1908.11391](#)].
- [126] G. Janssen et al., *Gravitational wave astronomy with the SKA*, *PoS AASKA14* (2015) 037, [[arXiv:1501.00127](#)].
- [127] G. Hobbs, A. Archibald, Z. Arzoumanian, D. Backer, M. Bailes, N. D. R. Bhat, M. Burgay, S. Burke-Spolaor, D. Champion, I. Cognard, and et al., *The international pulsar timing array project: using pulsars as a gravitational wave detector*, *Classical and Quantum Gravity* **27** (Apr, 2010) 084013.
- [128] J. Garcia-Bellido, H. Murayama, and G. White, *Exploring the Early Universe with Gaia and THEIA*, [arXiv:2104.04778](#).
- [129] M. Maggiore, *Gravitational wave experiments and early universe cosmology*, *Phys. Rept.* **331** (2000) 283–367, [[gr-qc/9909001](#)].

- [130] B. Allen and J. D. Romano, *Detecting a stochastic background of gravitational radiation: Signal processing strategies and sensitivities*, *Phys. Rev. D* **59** (1999) 102001, [[gr-qc/9710117](#)].
- [131] K. Schmitz, *New Sensitivity Curves for Gravitational-Wave Signals from Cosmological Phase Transitions*, *JHEP* **01** (2021) 097, [[arXiv:2002.04615](#)].
- [132] R. Blumenhagen, M. Cvetič, and T. Weigand, *Spacetime instanton corrections in 4D string vacua: The Seesaw mechanism for D-Brane models*, *Nucl. Phys. B* **771** (2007) 113–142, [[hep-th/0609191](#)].
- [133] B. Florea, S. Kachru, J. McGreevy, and N. Saulina, *Stringy Instantons and Quiver Gauge Theories*, *JHEP* **05** (2007) 024, [[hep-th/0610003](#)].
- [134] R. Blumenhagen, M. Cvetič, S. Kachru, and T. Weigand, *D-Brane Instantons in Type II Orientifolds*, *Ann. Rev. Nucl. Part. Sci.* **59** (2009) 269–296, [[arXiv:0902.3251](#)].
- [135] S. B. Giddings and A. Strominger, *Axion Induced Topology Change in Quantum Gravity and String Theory*, *Nucl. Phys. B* **306** (1988) 890–907.
- [136] K.-M. Lee, *Wormholes and Goldstone Bosons*, *Phys. Rev. Lett.* **61** (1988) 263–266.
- [137] L. F. Abbott and M. B. Wise, *Wormholes and Global Symmetries*, *Nucl. Phys. B* **325** (1989) 687–704.
- [138] S. R. Coleman and K.-M. Lee, *WORMHOLES MADE WITHOUT MASSLESS MATTER FIELDS*, *Nucl. Phys. B* **329** (1990) 387–409.
- [139] S. M. Barr and D. Seckel, *Planck scale corrections to axion models*, *Phys. Rev. D* **46** (1992) 539–549.
- [140] A. G. Dias, V. Pleitez, and M. D. Tonasse, *Naturally light invisible axion in models with large local discrete symmetries*, *Phys. Rev. D* **67** (2003) 095008, [[hep-ph/0211107](#)].
- [141] L. M. Carpenter, M. Dine, and G. Festuccia, *Dynamics of the Peccei Quinn Scale*, *Phys. Rev. D* **80** (2009) 125017, [[arXiv:0906.1273](#)].